JACS
JOURNAL OF THE AMERICAN CHEMICAL SOCIETY

Article

pubs.acs.org/JACS

# Targeted Catalytic Inactivation of Angiotensin Converting Enzyme by Lisinopril-Coupled Transition-Metal Chelates

Jeff C. Joyner,[†,‡] Lalintip Hocharoen,[†] and J. A. Cowan*[,†,‡,§]

[†]Evans Laboratory of Chemistry, The Ohio State University, 100 West 18th Avenue, Columbus, Ohio 43210, United States
[‡]The Ohio State Biochemistry Program, 784 Biological Sciences, 484 West 12th Avenue, Columbus, Ohio 43210, United States
[§]MetalloPharm LLC, 1790 Riverstone Drive, Delaware, Ohio 43015, United States

Supporting Information

**ABSTRACT:** A series of compounds that target reactive transition-metal chelates to somatic angiotensin converting enzyme (sACE-1) have been synthesized. Half-maximal inhibitory concentrations ($IC_{50}$) and rate constants for both inactivation and cleavage of full-length sACE-1 have been determined and evaluated in terms of metal chelate size, charge, reduction potential, coordination unsaturation, and coreactant selectivity. Ethylenediaminetetraacetic acid (EDTA), nitrilotriacetic acid (NTA), 1,4,7,10-tetraazacyclododecane-1,4,7,10-tetraacetic acid (DOTA), and tripeptide GGH were linked to the lysine side chain of lisinopril by 1-ethyl-3-[3-(dimethylamino)propyl]carbodiimide hydrochloride/*N*-hydroxysuccinimide coupling. The resulting amide-linked chelate−lisinopril (EDTA−lisinopril, NTA−lisinopril, DOTA−lisinopril, and GGH−lisinopril) conjugates were used to form coordination complexes with iron, cobalt, nickel, and copper, such that lisinopril could mediate localization of the reactive metal chelates to sACE-1. ACE activity was assayed by monitoring cleavage of the fluorogenic substrate Mca-RPPGFSAFK(Dnp)-OH, a derivative of bradykinin, following preincubation with metal chelate−lisinopril compounds. Concentration-dependent inhibition of sACE-1 by metal chelate−lisinopril complexes revealed $IC_{50}$ values ranging from 44 to 4500 nM for Ni−NTA−lisinopril and Ni−DOTA−lisinopril, respectively, versus 1.9 nM for lisinopril. Stronger inhibition was correlated with smaller size and lower negative charge of the attached metal chelates. Time-dependent inactivation of sACE-1 by metal chelate−lisinopril complexes revealed a remarkable range of catalytic activities, with second-order rate constants as high as 150 000 $M^{-1}$ $min^{-1}$ (Cu−GGH−lisinopril), while catalyst-mediated cleavage of sACE-1 typically occurred at much lower rates, indicating that inactivation arose primarily from side chain modification. Optimal inactivation of sACE-1 was observed when the reduction potential for the metal center was poised near 1000 mV, reflecting the difficulty of protein oxidation. This class of metal chelate−lisinopril complexes possesses a range of high-affinity binding to ACE, introduces the advantage of irreversible catalytic turnover, and marks an important step toward the development of multiple-turnover drugs for selective inactivation of sACE-1.

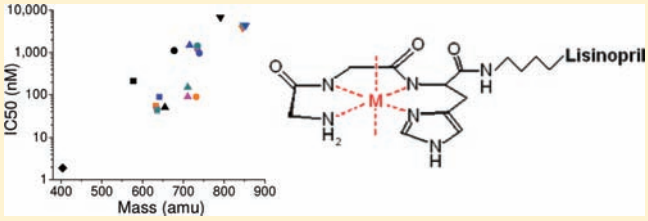


## INTRODUCTION

Angiotensin converting enzyme (ACE) is an important therapeutic target for treatment of hypertension and heart failure because of its critical physiological role in cardiovascular function, primarily the hydrolysis of angiotensin I to form angiotensin II, which results in vasoconstriction, and hydrolysis of the vasodilator bradykinin.[1−4] Human ACE-1 exists in multiple active forms: somatic ACE (sACE-1), a full-length two-domain (N and C) membrane-anchored enzyme, testicular ACE (tACE), a membrane-anchored enzyme with sequence identical to that of the C-terminal domain of sACE-1 (except for an additional N-terminal 36 amino acid segment),[5] and the N-domain form, a diffusible N-terminal cleavage product of sACE-1.[6,7] The N- and C-terminal domains share ∼60% sequence homology, similar active site structures,[5,6] similar substrate-binding selectivity,[2] and the requirement for an active site zinc cation for activity. Several inhibitors of sACE-1, such as lisinopril (currently marketed as Zestril and Prinivil), successfully alleviate hypertension and congestive heart failure, resulting in decreased mortality among patients,[1,8] by directly competing with the natural substrates for binding to sACE-1 active sites, resulting in overall vasodilation.

One significant limitation of lisinopril, and reversible inhibitors in general, is the requirement for stoichiometric saturation of the target; a typical active dose of lisinopril ranges from 5 to 40 mg for humans.[1] There is significant interest in the development of multiple-turnover drugs that irreversibly modify therapeutic targets, allowing substoichiometric concentrations of drug to be used with the potential for therapeutic effect at lower dosage with reduced side effects.[9−14] To this end, several research groups have recently developed various metallodrugs and/or artificial proteases that use target-selective metal catalysts, including hydrolytic Co− and Cu−cyclen, oxidative Ni− and Cu−ATCUN (ATCUN = amino terminal Cu- and Ni-binding), and photoactivated Ru complexes, to

**Received:** September 18, 2011
**Published:** December 24, 2011

  

effect protein modification.[9,10,13,15−25] The goal of this study was to develop a class of multiple-turnover metallodrugs that selectively and irreversibly inactivate sACE-1 using a variety of oxidative metal catalysts, with lisinopril as the targeting molecule.

A series of metallodrugs was developed in which transition-metal chelates (M−chelates) with known ability to generate reactive oxygen species with multiple turnovers[26] were attached to the lysine side chain of lisinopril, such that the inhibitor lisinopril targeted each reactive M−chelate to the active sites of sACE-1. The M−chelates used were based on combinations of the transition metals $Fe^{3+}$, $Co^{2+}$, $Ni^{2+}$, and $Cu^{2+}$ and the chelators 1,4,7,10-tetraazacyclododecane-1,4,7,10-tetraacetic acid (DOTA), ethylenediaminetetraacetic acid (EDTA), nitrilotriacetic acid (NTA), and tripeptide GGH. These complexes provided variability in reduction potential, coordination unsaturation, size, and charge.[12] The ability of each M−chelate−lisinopril complex to both reversibly inhibit and catalytically inactivate sACE-1 was assessed, and varying binding affinities and rates of targeted irreversible inactivation (and cleavage) of full-length sACE-1 by M−chelate−lisinopril complexes were observed. This class of compounds illustrates the potential for catalytic irreversible inactivation of sACE-1 as an efficient alternative to reversible inhibition and demonstrates that catalyst parameters such as reduction potential, coordination unsaturation, geometric alignment, size, and charge may be tuned to optimize catalytic efficiency. The results of this study are likely to prove valuable in the design and development of catalytic metallodrugs directed toward other therapeutic targets.

## MATERIALS AND METHODS

**Chemicals and Reagents.** Lisinopril was purchased from Cayman Chemical Co. and stored at −20 °C in powder form, and electrospray ionization time-of-flight MS (ESI-TOF-MS) analysis confirmed the expected mass of 404 amu. Recombinant human sACE-1 (Leu30−Leu1261, with a C-terminal His tag, >95% purity by sodium dodecyl sulfate−polyacrylamide gel electrophoresis (SDS−PAGE) under reducing conditions), originally isolated from an NS0-derived murine myeloma cell line, was purchased from R&D Systems as a stock solution containing 12.5 mM tris(hydroxymethyl)aminomethane (Tris), 75 mM NaCl, 0.5 μM $ZnCl_2$, and 40% (v/v) glycerol, pH 7.5, with [sACE-1] = 0.434 mg/mL, and divided into single-use aliquots prior to storage at −20 °C. Fluorogenic substrate Mca-RPPGFSAFK(Dnp)-OH was purchased from R&D Systems, dissolved in dimethyl sulfoxide (DMSO), divided into single-use aliquots, and stored at −20 °C. The bifunctional compound *N*-hydroxysuccinimide (NHS)−DOTA was purchased from Macrocyclics and stored at −20 °C in powder form. NHS was purchased from GenScript, and 1-ethyl-3-[3-(dimethylamino)propyl]carbodiimide hydrochloride (EDC) was purchased from Pierce and stored at −20 °C. EDTA was purchased from Aldrich. NTA was purchased from Sigma. The tripeptides GGH-OH (GGH) and Z-GGH-OH (Z-GGH; Z = carboxybenzyl) were obtained from Bachem, and DOTA was purchased from Macrocyclics. The iron(II) sulfate heptahydrate, cobalt(II) chloride hexahydrate, nickel(II) acetate tetrahydrate, copper(II) chloride dihydrate, and zinc(II) chloride salts were purchased from ACROS, J. T. Baker, Aldrich, J. T. Baker, and MCB Reagents, respectively. Sodium chloride, sodium hydroxide, and ammonium persulfate were purchased from Fisher. *N*-(2-Hydroxyethyl)piperazine-*N*′-ethanesulfonic acid (HEPES) was purchased from Sigma. Acetonitrile, SDS, and $Na_2HPO_4$ were purchased from Sigma-Aldrich, $NaHCO_3$ was purchased from Mallinckrodt, 40% acrylamide/bisacrylamide solution (19:1) was purchased from Bio-Rad, and trifluoroacetic acid (TFA) was purchased from ACROS. The silver stain kit was purchased from Pierce. The C18 preparatory and analytical columns used for reversed-phase HPLC (RP-HPLC) were purchased from Vydac, and the PolyWAX LP column used for anion exchange HPLC was purchased from PolyLC. $D_2O$ (99.96%) for $^1H$ NMR was purchased from Cambridge Isotopes Laboratory.

**Synthesis and Characterization.** Compound EDTA−lisinopril was prepared by making a solution containing 500 mM EDTA, 500 mM NHS, and 500 mM EDC in DMSO and reacting the solution for 20 min at ambient temperature. After 20 min, 48 μL of this reaction mixture was mixed with 552 μL of a solution that contained 22 mM lisinopril in 100 mM $NaHCO_3$, pH 8.0. The reaction proceeded overnight at room temperature (rt) in the dark, followed directly by anion exchange HPLC purification. Anion exchange elution conditions used a gradient method, running from 0% to 100% B from 0 to 50 min and at 100% B from 50 to 55 min, where mobile phase A is 10 mM $Na_2HPO_4$, pH 5.7, and B is 1 M NaCl, 10 mM $Na_2HPO_4$, pH 5.7. The anion exchange HPLC fraction for product EDTA−lisinopril was collected and further separated by RP-HPLC. RP-HPLC elution conditions used a gradient method, running from 15% to 65% B from 0 to 45 min, from 65% to 95% B from 45 to 50 min, and at 95% B from 50 to 55 min, where mobile phase A is $H_2O$, 0.1% TFA, and B is acetonitrile, 0.1% TFA. The RP-HPLC fraction for product EDTA−lisinopril was collected, lyophilized, and resuspended in water, and ESI-TOF-MS analysis provided the expected mass of 678 amu (negative mode), as well as the $+Na^+ - 1H^+$ adduct at 700 amu, with no evidence of uncoupled lisinopril reactant (404 amu). The EDTA−lisinopril concentration was quantified via UV/vis (270 nm) titration with a solution of known concentration of copper(II) chloride.

Compound NTA−lisinopril was prepared by making a solution containing 500 mM NTA, 500 mM NHS, and 500 mM EDC in DMSO and reacting the solution for 20 min, after which time 48 μL of the reaction volume was mixed with 552 μL of a solution that contained 22 mM lisinopril in 100 mM $NaHCO_3$, pH 8.0. The reaction proceeded overnight at rt in the dark, followed by consecutive HPLC purification (first anion exchange HPLC and then RP-HPLC) using the same elution conditions as used for EDTA−lisinopril. The RP-HPLC fraction for product NTA−lisinopril was collected, lyophilized, and resuspended in water, and ESI-LCQ-MS analysis (in the laboratory of Dr. Michael Freitas) provided the expected mass of 578 amu (negative mode), with no evidence of uncoupled lisinopril reactant. The NTA−lisinopril concentration was quantified via UV/vis (250 nm) titration with a solution of known concentration of iron(II) sulfate.

Compound DOTA−lisinopril was prepared by making a solution containing 40 mM NHS−DOTA (10× stock made in DMSO) and 20 mM lisinopril in 100 mM $NaHCO_3$, pH 8.0. The reaction proceeded overnight at rt in the dark, followed by consecutive HPLC purification (first anion exchange HPLC and then RP-HPLC) using the same elution conditions as used for EDTA−lisinopril. The RP-HPLC fraction for product DOTA−lisinopril was collected, lyophilized, and resuspended in water, and ESI-TOF-MS analysis provided the expected mass of 791 amu (negative mode), with no evidence of uncoupled lisinopril reactant. The DOTA−lisinopril concentration was quantified via UV/vis (240 nm) titration with a solution of known concentration of nickel(II) acetate.

Compound GGH−lisinopril was prepared by making a solution containing 200 mM Z-GGH, 200 mM NHS, and 200 mM EDC in DMSO and reacting the solution for 20 min, after which time 54 μL of this reaction volume was mixed with 30 μL of 200 mM lisinopril in DMSO. The reaction proceeded overnight at rt in the dark, followed by consecutive HPLC purification (first anion exchange HPLC and then RP-HPLC) using the same elution conditions as used for EDTA−lisinopril. The RP-HPLC fraction for product Z-GGH−lisinopril was collected and lyophilized. ESI-TOF-MS analysis provided the expected mass for Z-GGH−lisinopril of 789 amu with no evidence of uncoupled lisinopril reactant. The lyophilized Z-GGH−lisinopril was deprotected by being dissolved in 1 mL of TFA, and 5 mg of 20% $Pd(OH)_2$ on charcoal was added and the resulting mixture stirred to form a slurry. The mixture was Ar-purged, and the anaerobic solution was reacted under a positive pressure of $H_2$ for ∼6 h. The mixture was dried under vacuum, redissolved in water, and centrifuged to remove solid catalyst, and the resulting deprotected


dx.doi.org/10.1021/ja208791f | J. Am. Chem. Soc. 2012, 134, 3396−3410

GGH−lisinopril was purified by RP-HPLC using the same RP-HPLC conditions as used for EDTA−lisinopril. The RP-HPLC fraction for product GGH−lisinopril was collected, lyophilized, and resuspended in water, and ESI-TOF-MS analysis provided the expected mass of 655 amu (negative mode), as well as the $+Na^+ - 1H^+$ adduct at 677 amu, with no evidence of uncoupled lisinopril reactant. The concentration of product GGH−lisinopril was quantified via UV/vis (245 nm) titration with a solution of known concentration of nickel(II) acetate.

The identities and isomeric purity of the synthesized chelate−lisinopril compounds were validated by $^1$H NMR analysis, analytical RP-HPLC, and ESI-MS (Figures SM1−SM19, Supporting Information). Divalent iron, cobalt, nickel, and copper complexes of DOTA−lisinopril, EDTA−lisinopril, NTA−lisinopril, and GGH−lisinopril were prepared by mixing the respective metal salts with the chelate−lisinopril species in a buffer containing 20 mM HEPES, 100 mM NaCl, pH 7.4, and incubating the mixtures at rt for 30 min prior to each measurement. M−chelate complex formation was verified by metal ion titration monitored by UV/vis (Figures SM20−SM23, Supporting Information). Metal:chelate ratios of 1:1 and 1:1.1 (to ensure that essentially all metal was chelated) were used for concentration-dependent and time-dependent inactivation experiments, respectively. The $Fe^{2+}$ complex with GGH−lisinopril was not used in later experiments due to weak complex formation. Experimentally determined extinction coefficients for all M−chelate−lisinopril and M−chelate species, as well as stability constants for M−chelates, are summarized in the Supporting Information (Tables SM1 and SM2).

**Determination of $IC_{50}$ Values.** sACE-1 (1 nM) and variable concentrations of each M−chelate−lisinopril complex (prepared in the absence of $Zn^{2+}$) were incubated for 20 min at 37 °C in a buffer containing 50 mM HEPES, 300 mM NaCl, 10 μM $ZnCl_2$, 0.05% Brij35, pH 7.4. After 20 min, 68.6 μL of each preincubated mixture of sACE-1 and inhibitor was mixed with 1.4 μL of 0.5 mM fluorogenic substrate in a fluorescence cuvette, and substrate cleavage by sACE-1 was immediately monitored by real-time fluorimetry at 37 °C, with excitation at 320 nm and emission at 405 nm. Initial rates of fluorescence increase were determined for each concentration of M−chelate−lisinopril, and these initial rates were expressed as a percentage (percentage of maximal activity) of the average of several initial rates of uninhibited substrate cleavage by sACE-1 in the absence of M−chelate−lisinopril complexes. Plots of the percentage of maximal activity vs the M−chelate−lisinopril concentration were fit

$$A = (100\%)/[1 + ([I]/[IC_{50}])^n] \quad (1)$$

to eq 1, where $A$, [I], $n$, and [$IC_{50}$] are the percentage of maximal activity, inhibitor concentration, fitted cooperativity, and fitted $IC_{50}$, respectively. $IC_{50}$ values were determined for each M−chelate−lisinopril, chelate−lisinopril, M−chelate, and chelator species.

**Time-Dependent Inactivation of sACE-1.** sACE-1 and each M−chelate−lisinopril complex (prepared in the absence of $Zn^{2+}$) were preincubated for 20 min at 37 °C in a buffer containing 50 mM HEPES, 300 mM NaCl, 10 μM $ZnCl_2$, 0.05% Brij35, pH 7.4, and after 20 min, coreactants ascorbate and/or $H_2O_2$ (or no coreactants) were added to initiate each reaction. The reaction concentrations were 1 nM sACE-1, a concentration of M−chelate−lisinopril that gave approximately 80% activity (calculated by use of eq 1, where $A$ = 80%, concentrations listed in Table 1) and 1 mM ascorbate and/or $H_2O_2$ (or no coreactants). Each time-dependent ACE-inactivation reaction proceeded at 37 °C for a period of 2 h, and at each specific intervening time point, a 68.6 μL aliquot of the reaction mixture containing sACE-1 was mixed with 1.4 μL of 0.5 mM fluorogenic substrate in a fluorescence cuvette. Substrate cleavage by sACE-1 was immediately monitored by real-time fluorimetry at 37 °C, with excitation at 320 nm and emission at 405 nm. Initial rates were determined for each time point for the time-dependent inactivation of sACE-1, and these initial rates were expressed as a percentage (percentage of maximal activity) of the average of several initial rates for uninhibited substrate cleavage by sACE-1, determined in the absence of both M−chelate−lisinopril complexes and coreactants. Plots of the percentage of maximal activity vs time were fit to a first-order exponential decay model, and initial rates of inactivation of sACE-1 by M−chelate−lisinopril complexes were determined. Second-order rate constants for inactivation of

$$k_2 = R/([I]\cdot[E]) \quad (2)$$

sACE-1 were obtained using eq 2, where $k_2$ is the second-order rate constant ($M^{-1}$ $min^{-1}$), $R$ is the initial rate of enzyme inactivation (M/min) after subtraction of the corresponding background rate in the absence of M−chelate−lisinopril complex, but with the same coreactants, [I] is the concentration of M−chelate−lisinopril complex used (M), and [E] is the concentration of sACE-1 used ($1 \times 10^{-9}$ M). Control experiments with M−chelate complexes lacking attached lisinopril were performed in the same manner and conditions used for the respective M−chelate−lisinopril complexes.

**Characterization of Residual Activity for Inactivated sACE-1.** sACE-1 (1 nM), $H_2O_2$ (1 mM), ascorbate (1 mM), and each M−chelate−lisinopril ($IC_{20}$ concentration) were preincubated for 15 h at 37 °C. Following preincubation, 68.6 μL aliquots of the reaction mixture containing inactivated sACE-1 were separately mixed with 1.4 μL of variable concentrations of fluorogenic substrate in a fluorescence cuvette at 37 °C. Substrate cleavage by sACE-1 was immediately monitored by real-time fluorimetry, and initial rates (fluorescence intensity per minute) were recorded. The inner-filter effect for the fluorogenic substrate, which became significant at higher substrate

$$F_{corr} = F_{obsd}\cdot 10^{[(\varepsilon_{ex}l_{ex}+\varepsilon_{em}l_{em})\cdot c/2]} \quad (3)$$

concentrations, was corrected for by use of eq 3,[27] where $c$ is the concentration of substrate, $F_{obsd}$ and $F_{corr}$ are the uncorrected and corrected fluorescence intensities, respectively, $l_{ex}$ and $l_{em}$ are the fluorescence cuvette path lengths for excitation and emission, respectively, and $\varepsilon_{ex}$ and $\varepsilon_{em}$ are the fluorogenic substrate extinction coefficients at 320 and 405 nm, respectively. Initial rate units of corrected fluorescence intensity per minute were converted to units of micromolar substrate per minute through use of a linear standard curve, which related the total change in fluorescence intensity resulting from complete substrate cleavage to the substrate concentration used. Plots of initial rate (μM substrate/min) vs substrate concentration (μM) were constructed and were fit to the Michaelis−Menten equation to obtain $k_{cat}$, $K_M$, and $k_{cat}/K_M$ values for inactivated sACE-1. Metal complex preparation, complex concentration, and preincubation conditions were the same as used in the time-dependent inactivation assay.

**SDS−PAGE Analysis.** sACE-1 (20 nM), $H_2O_2$ (1 mM), ascorbate (1 mM), and each M−chelate−lisinopril complex (concentration that gave 20% saturation of 20 nM sACE-1, ~$IC_{50}$/4) were preincubated for 15 h at 37 °C. The resulting mixtures were separated by 7.5% SDS−PAGE, and silver staining was used to visualize sACE-1 and cleavage products. To quantify the sACE-1 remaining after each time-dependent incubation reaction, the intensity of each starting material band was quantified and converted to the percentage of full-length sACE-1 remaining. Initial rates of cleavage of sACE-1 were determined by incubating M−chelate−lisinopril complexes, coreactants, and sACE-1 for varied time intervals (0, 10, 20, 50, and 80 min) and fitting of the change in the percentage of full-length sACE-1 remaining over time to a first-order equation; these initial rates were expressed as the percentage of full-length sACE-1 per minute. In the case of the 15 h incubation reactions, the concentrations (mol %) of full-length sACE-1 and each cleavage product were determined by use of the intensities of each band and apparent molecular weights. Control reactions were also performed for reactions with M−chelates lacking attached lisinopril, as well as for reactions lacking catalyst, coreactants, or both (Figures SM34, SM37, and SM38 and Table SM5, Supporting Information).

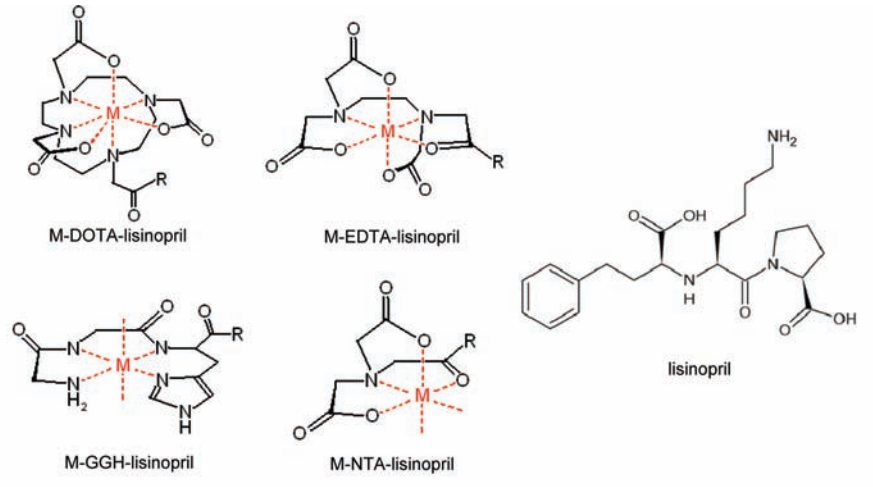


**Figure 1.** Summary of the metal chelate complexes and their attachment to the lysine side chain of lisinopril. M = $Fe^{3+}$, $Co^{2+}$, $Ni^{2+}$, $Cu^{2+}$; R = N(H)-lisinopril.

**Molecular Modeling.** Interactions between both the N- and C-domains of sACE-1 and the M−chelate−lisinopril complexes were modeled using a combination of Spartan and Gaussian software. From the X-ray crystal structure of the N-domain of sACE-1 in complex with the inhibitor lisinopril (PDB ID 2C6N), a sphere with 15 Å radius, centered on the N atom of the lisinopril lysine side chain, was generated in Gaussian and used to model the active site. This process was repeated using the X-ray crystal structure of the C-domain of ACE (tACE) in complex with lisinopril (PDB ID 1O86). Molecular mechanics energy minimization was performed in Spartan using the Merck molecular force field MMFFaq, in which structural energy minimization occurred without solvent considerations. Model geometries were constrained to the X-ray crystal structures, while the lisinopril lysine side chain and lysine−chelate linker geometries were allowed to vary during energy minimization. Structures were accepted once 10 successive rounds of energy minimization lowered the energy by no more than 0.1 kcal/mol. Modeling parameters: equilibrium geometry at the ground state, subject to frozen atoms and symmetry, multiplicity singlet, total charge 0 (partial charges handled by MMFFaq[28]). Gaussian software was used to generate figures.

**Complex Kinetic Stability.** To observe whether $Zn^{2+}$ was able to displace each transition metal from each chelate, a solution containing 100 $\mu$M M−chelate complex and 100 $\mu$M $ZnCl_2$ was incubated at 37 °C (in a cuvette) in a buffer containing 20 mM HEPES, 100 mM NaCl, pH 7.4, and a UV/vis scan (from 800 to 200 nm) was taken every 1.5 min. This process was repeated for each M−chelate used, and the rate of the transition (if present) from M−chelate + $Zn^{2+}$ to $Zn^{2+}$−chelate + metal was determined by following the change in absorbance at the specified wavelengths for each M−chelate over time (Figure SM40 and Table SM7, Supporting Information).

## RESULTS

**Synthesis and Characterization.** Chelate−lisinopril conjugates (DOTA−lisinopril, EDTA−lisinopril, GGH−lisinopril, and NTA−lisinopril) were synthesized by coupling the respective chelators with the lysine side chain of lisinopril to form amide linkages. Synthesis of DOTA−lisinopril was achieved by direct reaction of lisinopril with the bifunctional chelator NHS−DOTA. Syntheses of both EDTA−lisinopril and NTA−lisinopril were each performed by activation of EDTA and NTA with EDC/NHS in DMSO, followed by addition of a limiting concentration of lisinopril. Synthesis of GGH−lisinopril was achieved in three steps. First, Z-GGH was reacted with EDC/NHS in DMSO to form the activated NHS ester of Z-GGH. Second, a limiting concentration of lisinopril was added (in DMSO) to form the product Z-GGH−lisinopril. Catalytic hydrogenation over $Pd(OH)_2/C$ in TFA yielded the final deprotected product GGH−lisinopril.

Separation of chelate−lisinopril species from reactants was generally achieved by two consecutive HPLC steps. First, chelate−lisinopril products were isolated by anion exchange HPLC, and second, anion exchange fractions containing product were purified by RP-HPLC. RP-HPLC alone was generally not sufficient to effect adequate separation, because the RP-HPLC chelate−lisinopril elution times were too similar to that of lisinopril (with the exception of Z-GGH−lisinopril, which differed in elution time from lisinopril by 7 min), whereas anion exchange allowed separation of NTA−lisinopril, EDTA−lisinopril, and DOTA−lisinopril from the lisinopril reactant by at least 12 min in elution time. Subsequent purification by RP-HPLC allowed separation from any remaining free chelator or other reactants (by at least 10 min) and simultaneously served to desalt the chelate−lisinopril products. Following synthesis and HPLC purification, mass spectrometric analysis revealed the expected masses for EDTA−lisinopril, NTA−lisinopril, DOTA−lisinopril, and GGH−lisinopril (678, 578, 791, and 655 amu, respectively) with no observed mass for remaining uncoupled lisinopril (404 amu) in any of the products. $^1$H NMR analysis confirmed the identity and isomeric purity of the synthesized products.

Complex formation between each metal ion ($Fe^{2+}$, $Co^{2+}$, $Ni^{2+}$, and $Cu^{2+}$) and each chelator−lisinopril species, as well as each chelator lacking lisinopril, was monitored by UV/vis spectroscopy, and metal complex extinction coefficients were determined. As expected, complex formation between $Fe^{2+}$ and GGH was not observed under the experimental conditions used, so the combination of $Fe^{2+}$ with GGH−lisinopril was not used in later experiments. $Fe^{2+}$ is known to convert to $Fe^{3+}$ following chelation under the aerobic conditions used in this study; therefore, the 3+ oxidation state of iron complexes of NTA−lisinopril, EDTA−lisinopril, and DOTA−lisinopril differed from the 2+ oxidation state of the other metal complexes. Absorption spectra for each of the M−chelate−lisinopril species closely matched the characteristic absorption spectra for each of the respective M−chelates obtained without the attached lisinopril, although the extinction coefficients for the charge transfer bands of Fe−DOTA and Cu−NTA were observed to decrease and increase, respectively, following


dx.doi.org/10.1021/ja208791f | J. Am. Chem. Soc. 2012, 134, 3396−3410

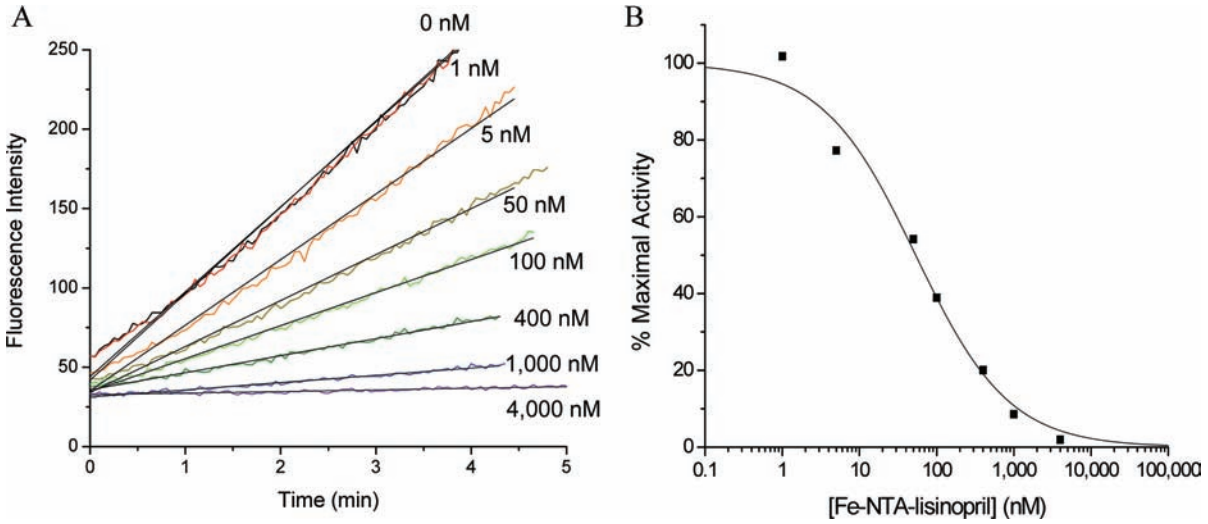


**Figure 2.** Concentration-dependent inactivation of sACE-1 by Fe−NTA−lisinopril. (A) sACE-1 (1 nM) was preincubated with variable concentrations of Fe−NTA−lisinopril, and subsequently, the sACE-1 activity was measured from the initial cleavage rates of fluorogenic substrate. (B) Dependence of sACE-1 activity on Fe−NTA−lisinopril concentration. $IC_{50}$ values were determined for all synthesized M−chelate−lisinopril complexes in the same manner.

coupling to lisinopril. The M−chelate−lisinopril species used in this study are summarized in Figure 1.

**Concentration-Dependent Inhibition of sACE-1.** The relative binding affinity of each M−chelate−lisinopril species to sACE-1, as well as other species lacking metal, lisinopril, or both, was determined by incubating the enzyme with variable concentrations of each inhibitor and following the change in rate for sACE-1-mediated cleavage of the fluorogenic substrate Mca-RPPGFSAFK(Dnp)-OH (Figure 2). $IC_{50}$ values for sACE-1 inhibition were determined for each complex and are summarized in Table 1. Lisinopril was found to have an $IC_{50}$ of 1.9 nM, consistent with previous reports.[29] Following attachment of M−chelates to lisinopril, $IC_{50}$ values were found in the range of 44−4500 nM, with $IC_{50}$ values increasing (affinity decreasing) in the order M−NTA−lisinopril < M−GGH−lisinopril ≈ M−EDTA−lisinopril < M−DOTA−lisinopril. These results confirm the expected inverse correlation between target affinity and steric bulk, as well as negative charge, of the attached M−chelate.[29] Among metals, it was generally found that Fe complexes had the lowest $IC_{50}$ values, most likely reflecting the trivalent oxidation state of iron and the higher positive charge associated with the resulting complex, consistent with the inverse correlation observed between the overall negative charge on the chelate−lisinopril complex and affinity for sACE-1. Experiments in which both inhibitor concentration and substrate concentration were varied were performed for lisinopril and Cu−GGH−lisinopril, and these experiments confirm a competitive mode of inhibition of sACE-1, with active site binding (Dixon plots shown in Figure SM27, Supporting Information).

Comparison of $IC_{50}$ values obtained for M−chelate−lisinopril complexes with those obtained for M−chelates lacking lisinopril confirms the requirement for lisinopril to direct the attached M−chelates to the sACE-1 active sites. Weak inhibition of sACE-1 by M−chelates alone presumably reflected weaker interactions with either sACE-1 or the substrate through metal coordination, hydrogen bonding, or electrostatic interactions, while strong inhibition of sACE-1 by M−chelate−lisinopril complexes resulted from specific binding to the active site. Weak inhibition was also observed for metal-free chelators, with $IC_{50}$ values ranging from 7000 to over 100 000 nM, and $IC_{50}$ values increased in the order DOTA < EDTA < NTA < GGH, although sACE-1 inhibition by metal-free chelators lacking lisinopril appeared to depend solely upon the ability of each chelator to bind $Zn^{2+}$ (present at 10 000 nM), a cofactor necessary for sACE-1 activity, rather than active site binding, consistent with prior investigations.[30,31] Chelation of $Zn^{2+}$ was expected to be much less prominent for metal-free GGH than for the metal-free chelators DOTA, EDTA, and NTA, as a result of the distinct mode of chelation for GGH,[32−34] and this was indeed reflected by the relatively high $IC_{50}$ for sACE-1 inhibition by metal-free GGH. In principle, metal-bound chelators also possess the potential to undergo slow exchange with active site $Zn^{2+}$, although such exchange was found to be insignificant under the conditions used, as discussed quantitatively in a later section. Following attachment of metal-free chelators to lisinopril, sACE-1 inhibition was enhanced by as much as 2000-fold (for GGH). In summary, attachment to lisinopril was a requirement for high-affinity targeting of M−chelates to the active sites of sACE-1, yielding a variety of ACE affinities that depended on the chemical nature of the M−chelate.

**Structural Modeling.** Molecular models were constructed to visually assess the alignment of M−chelate−lisinopril complexes within the active sites of ACE (Figure 3; Figure SM39, Supporting Information). Model geometries were constrained to that of the X-ray crystal structure of ACE (N- and C-domains, separately) in complex with lisinopril, while geometries for the lysine side chain of lisinopril and attached M−chelates were allowed to vary, and molecular mechanics energy minimization was performed. Structural models revealed that the M−DOTA portion of the M−DOTA−lisinopril complex preferred not to settle into the active sites of either the N-domain or C-domain of ACE, consistent with the relatively large size/charge of M−DOTA relative to M−EDTA, M−NTA, and M−GGH, as well as the relatively high $IC_{50}$ values observed for the M−DOTA−lisinopril complexes, while M−EDTA−lisinopril, M−NTA−lisinopril, and M−GGH−lisinopril all preferred complete burial of the respective M−chelates within the active sites of both the N- and C-domains of


dx.doi.org/10.1021/ja208791f | J. Am. Chem. Soc. 2012, 134, 3396−3410

**Table 1. $IC_{50}$ Values for sACE-1 Inhibition by Metal Chelate−Lisinopril Complexes, Metal Chelates, Chelator−Lisinopril Compounds, and Chelators**

| complex | $IC_{50}$ (nM) | TD concn[a] (nM) |
|---|---|---|
| $[NTA]^{2-}$−lisinopril | 210 ± 40 | *b* |
| $[Fe-NTA]^{+}$−lisinopril | 54 ± 9 | 7.8 |
| $[Co-NTA]^{0}$−lisinopril | 45 ± 8 | 4.8 |
| $[Ni-NTA]^{0}$−lisinopril | 44 ± 4 | 4.8 |
| $[Cu-NTA]^{0}$−lisinopril | 90 ± 10 | 15 |
| $[GGH]^{+}$−lisinopril | 50 ± 10 | *b* |
| $[Co-GGH]^{0}$−lisinopril | 90 ± 10 | 20 |
| $[Ni-GGH]^{0}$−lisinopril | 150 ± 30 | 25 |
| $[Cu-GGH]^{0}$−lisinopril | 1470 ± 20 | 300 |
| $[EDTA]^{3-}$−lisinopril | 1100 ± 100 | *b* |
| $[Fe-EDTA]^{0}$−lisinopril | 88 ± 5 | 14 |
| $[Co-EDTA]^{-}$−lisinopril | 1200 ± 40 | 210 |
| $[Ni-EDTA]^{-}$−lisinopril | 1420 ± 50 | 250 |
| $[Cu-EDTA]^{-}$−lisinopril | 960 ± 60 | 230 |
| $[DOTA]^{3-}$−lisinopril | 6800 ± 900 | *b* |
| $[Fe-DOTA]^{0}$−lisinopril | 3800 ± 400 | 870 |
| $[Co-DOTA]^{-}$−lisinopril | 4100 ± 200 | 790 |
| $[Ni-DOTA]^{-}$−lisinopril | 4500 ± 200 | 980 |
| $[Cu-DOTA]^{-}$−lisinopril | 4400 ± 400 | 1000 |
| lisinopril | 1.9 ± 0.3 | *b* |
| fluorescein−lisinopril | 290 ± 20 | *b* |
| DOTA | 7000 ± 1000 | *b* |
| $[Cu-DOTA]^{2-}$ | 30000 ± 2000 | *c* |
| EDTA | 7200 ± 600 | *b* |
| $[Cu-EDTA]^{2-}$ | 26000 ± 5000 | *c* |
| NTA | 32000 ± 3000 | *b* |
| $[Cu-NTA]^{-}$ | 36000 ± 4000 | *b* |
| GGH | >100000 | *b* |
| $[Cu-GGH]^{-}$ | 17000 ± 2000 | *c* |

[a]The concentration of M−chelate−lisinopril that inhibited sACE-1 by 20% (TD concn) was used in time-dependent sACE-1 inactivation experiments so that the remaining 80% activity could be used to monitor the kinetics of inactivation. The concentration required for 20% saturation was higher for cleavage assays, due to the higher concentration of sACE-1 used (20 nM). [b]A time-dependent inactivation experiment was not performed. [c]The concentration used for time-dependent inactivation was the same as that used for the corresponding M−chelate−lisinopril complex.

ACE. Several negatively charged residues of ACE (D140 for N-domain ACE; D377 and E162 for tACE) were positioned in close proximity to the M−chelate portion of the M−chelate−lisinopril complexes, and these residues most likely contribute to electrostatic repulsion of negatively charged M−chelates, while attracting positive functional groups, such as the lysine side chain of unmodified lisinopril. Additionally, many residues with known susceptibility to side chain oxidation (His, Pro, Arg, Lys, Thr, Tyr, Cys, Trp)[35,36] are positioned in this binding pocket. Several of these have known roles in binding and/or hydrolysis of ACE substrates, including binding of active site $Zn^{2+}$ (H361 and H365 in N-domain ACE; H383 and H387 in tACE) and $Cl^{-}$ ions (R186, W485, and R489 for chloride I and Y224 and R522 for chloride II in tACE; Y202 and Y501 for chloride II in N-domain ACE).[5,6] Oxidation of such residues is the most likely cause of the oxidative inactivation of ACE.

**Time-Dependent Inactivation of sACE-1.** The time-dependent catalytic inactivation of sACE-1 by each M−chelate−lisinopril complex was determined by incubating each complex with sACE-1 in the presence of coreactants and assaying the substrate cleavage activity of sACE-1 at various time intervals during the incubation (Figure 4A). Catalytic inactivation of sACE-1 promoted by each M−chelate−lisinopril complex was tested aerobically under a variety of coreactant conditions that included 1 mM ascorbate + 1 mM $H_2O_2$, 1 mM ascorbate, 1 mM $H_2O_2$, and with no added coreactants. For catalysts and conditions promoting above-background initial rates of inactivation of sACE-1, the initial rates of cleavage of full-length sACE-1 were determined by SDS−PAGE (Figure 4B,C). Comparisons between initial rates of inactivation and initial rates of protein cleavage (Table 2) allowed an assessment of whether the observed inactivation arose from either side chain modification or backbone cleavage. Initial rates of cleavage were significantly lower than the overall rates of inactivation, suggesting that the observed inactivation arose primarily from side chain oxidation, rather than backbone cleavage, except for several reactions with Fe− and Co−DOTA−lisinopril and Cu−GGH−lisinopril, for which the initial rate of cleavage was both >50% of the initial rate of inactivation and greater than the background rate of cleavage. The observed rates for both inactivation and cleavage of full-length sACE-1 by the redox-active M−chelate−lisinopril catalysts depended on the presence of a coreactant.

Catalytic inactivation of sACE-1 was observed for several M−chelate−lisinopril complexes, among which Cu−GGH−lisinopril was found to be the fastest. In the presence of both ascorbate and $H_2O_2$, rates of sACE-1 inactivation decreased in the order Cu−GGH−lisinopril > Fe−DOTA−lisinopril ≈ Ni−DOTA−lisinopril ≈ Cu−DOTA−lisinopril > Co−EDTA−lisinopril > Co−DOTA−lisinopril > Co−GGH−lisinopril ≈ Ni−GGH−lisinopril. In the presence of ascorbate (without $H_2O_2$), rates of sACE-1 inactivation decreased in the order Cu−GGH−lisinopril > Fe−EDTA−lisinopril > Co−DOTA−lisinopril ≈ Cu−DOTA−lisinopril ≈ Ni−GGH−lisinopril ≈ Cu−EDTA−lisinopril. In the presence of $H_2O_2$ (without ascorbate), rates of sACE-1 inactivation decreased in the order Fe−DOTA−lisinopril > Cu−GGH−lisinopril > Co−EDTA−lisinopril > Cu−EDTA−lisinopril ≈ Ni−DOTA−lisinopril. Control experiments were performed for M−chelates lacking attached lisinopril, and under these conditions the rates of sACE-1 inactivation were found to be dramatically reduced (generally at least 10-fold reduction), reflecting the requirement for lisinopril to promote targeted inactivation of sACE-1 (Table 4; Figure SM32, Supporting Information). Catalytic inactivation of sACE-1 by M−chelate−lisinopril complexes was generally dependent on the presence of a redox coreagent (ascorbate, $H_2O_2$, or $O_2$), each of which is physiologically available, and in most cases the combination of a reductant (ascorbate) with an oxidant ($O_2$ or $H_2O_2$) yielded the fastest rates of inactivation. The rate of sACE-1 inactivation in the absence of either M−chelate−lisinopril complex or coreactant was negligible, and no substrate cleavage was observed with catalyst and coreactants in the absence of enzyme (Figure SM33, Supporting Information). The initial rates of catalytic inactivation and cleavage of full-length sACE-1 by each M−chelate−lisinopril complex, under each set of coreactant conditions, as well as previously determined reduction potentials for each attached M−chelate,[12] are summarized in Table 2. All initial rates of inactivation are plotted in Figure 5 for visual comparison.

**Characterization of Inactivated sACE-1.** Incubation of sACE-1 with M−chelate−lisinopril complexes and coreactants typically reduced enzyme activity to a nonzero activity; residual


dx.doi.org/10.1021/ja208791f | J. Am. Chem. Soc. 2012, 134, 3396−3410

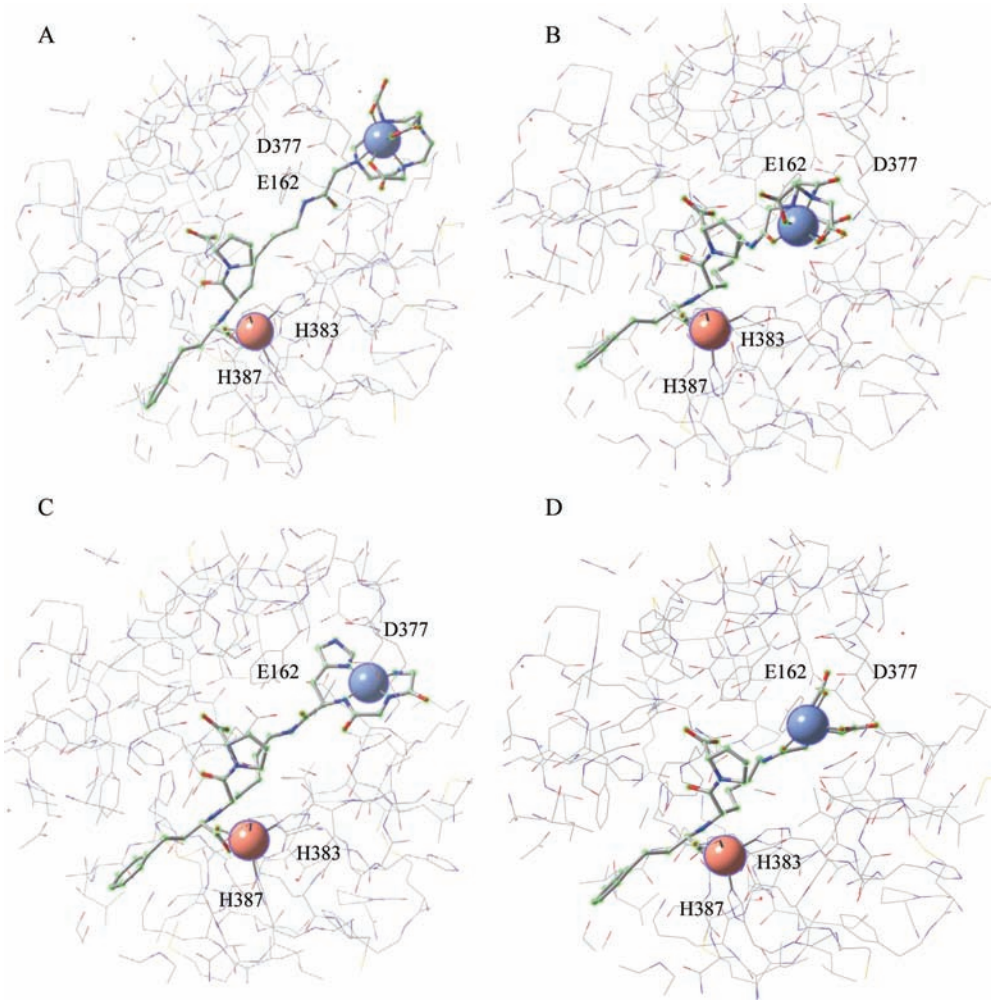


**Figure 3.** Energy-minimized structural models of the tACE active site (equivalent to the active site of the C-domain of sACE except for 36 additional residues at the N-terminus of tACE). The models show binding by (A) Fe−DOTA−lisinopril, (B) Fe−EDTA−lisinopril, (C) Cu−GGH−lisinopril, and (D) Fe−NTA−lisinopril. The redox-active metal for each metal chelate−lisinopril complex is shown as a blue sphere (upper right within each model), and the active site $Zn^{2+}$ is shown as a pink sphere (bottom left within each model). Residues E162 and D377 can interact with the lysine side chain of unmodified lisinopril, while H383 and H387 form part of the conserved HEXXH $Zn^{2+}$-binding motif.

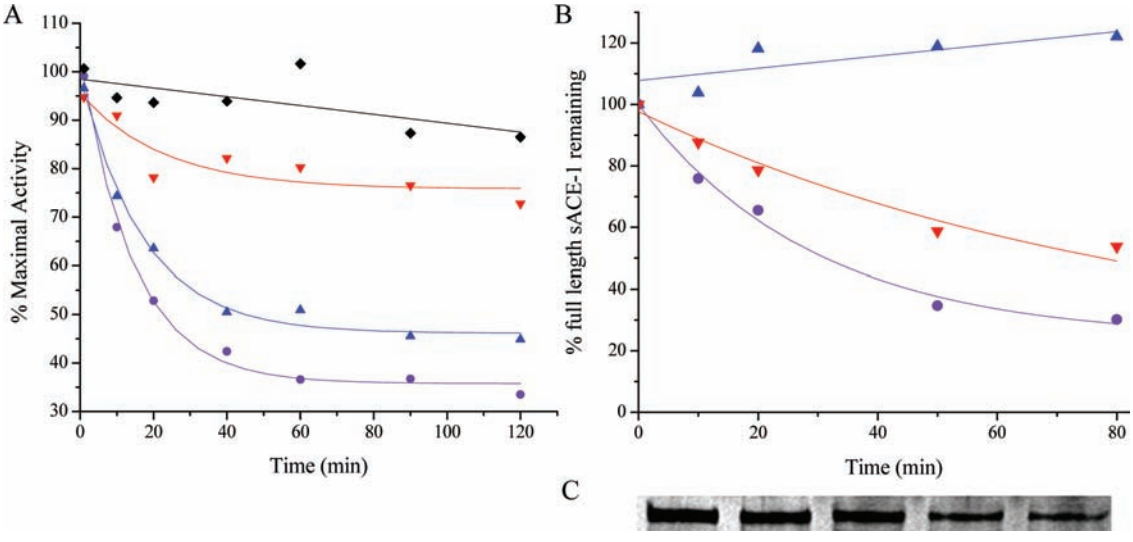


**Figure 4.** Time-dependent inactivation (A) and cleavage (B) of full-length sACE-1 by Cu−GGH−lisinopril with the coreactants 1 mM ascorbate and 1 mM $H_2O_2$ (●), 1 mM ascorbate (▲), and 1 mM $H_2O_2$ (▼) or no coreactant (◆). Time-dependent cleavage of sACE-1 was quantified by SDS−PAGE (C), shown here for the reaction of Cu−GGH−lisinopril with ascorbate and $H_2O_2$.


dx.doi.org/10.1021/ja208791f | J. Am. Chem. Soc. 2012, 134, 3396−3410

**Table 2. Initial Rates for Both Inactivation and Cleavage of Full-Length sACE-1 by M−Chelate−Lisinopril Complexes and Reduction Potentials of the Attached M−Chelates**

| | initial rates for inactivation {and cleavage} of full-length sACE-1 (% sACE-1/min) by M−chelate−lisinopril complexes and coreactants[b] | | | | |
|---|---|---|---|---|---|
| complex[a] | ascorbate + $H_2O_2$ | ascorbate | $H_2O_2$ | none | reduction potential vs NHE of M−chelate (mV)[c] |
| Fe−NTA−lisin | 0.06 ± 0.01 | 0.01 ± 0.02 | 0.01 ± 0.03 | 0.02 ± 0.02 | 464 |
| Co−NTA−lisin | 0.04 ± 0.04 | <0.03 | 0.01 ± 0.02 | 0.04 ± 0.04 | 274 |
| Ni−NTA−lisin | 0.09 ± 0.01 | <0.04 | <0.02 | <0.03 | 176 |
| Cu−NTA−lisin | 0.08 ± 0.02 | 0.03 ± 0.03 | 0.01 ± 0.03 | 0.03 ± 0.04 | 215 |
| Co−GGH−lisin | **0.24 ± 0.02** {< 0.2} | 0.07 ± 0.03 | <0.06 | 0.02 ± 0.03 | −119 |
| Ni−GGH−lisin | **0.20 ± 0.04** {< 0.05} | **0.11 ± 0.03** {0.12 ± 0.08} | 0.10 ± 0.05 | 0.04 ± 0.07 | 1000 |
| Cu−GGH−lisin | **4.7 ± 0.2** {2.6 ± 0.6} | **3.1 ± 0.2** {<0.09} | **0.9 ± 0.2** {0.6 ± 0.1} | 0.09 ± 0.04 | 1038 |
| Fe−EDTA−lisin | 0.07 ± 0.02 | **0.19 ± 0.03** {<0.1} | 0.03 ± 0.03 | 0.02 ± 0.04 | 391 |
| Co−EDTA−lisin | **0.6 ± 0.2** {< 0.08} | 0.05 ± 0.01 | **0.8 ± 0.2** {0.29 ± 0.09} | 0.03 ± 0.03 | 146 |
| Ni−EDTA−lisin | 0.07 ± 0.03 | 0.02 ± 0.02 | 0.05 ± 0.03 | 0.03 ± 0.02 | 172 |
| Cu−EDTA−lisin | 0.14 ± 0.02 | **0.10 ± 0.03** {0.28 ± 0.07} | **0.15 ± 0.06** {<0.09} | 0.06 ± 0.04 | 47 |
| Fe−DOTA−lisin | **0.75 ± 0.09** {0.43 ± 0.08} | 0.04 ± 0.02 | **1.9 ± 0.4** {<0.04} | 0.08 ± 0.03 | 396 |
| Co−DOTA−lisin | **0.51 ± 0.04** {0.4 ± 0.2} | **0.14 ± 0.05** {0.1 ± 0.1} | 0.04 ± 0.03 | 0.04 ± 0.03 | 142 |
| Ni−DOTA−lisin | **0.75 ± 0.08** {< 0.01} | 0.03 ± 0.02 | **0.13 ± 0.01** {<0.1} | 0.01 ± 0.04 | −35 |
| Cu−DOTA−lisin | **0.73 ± 0.03** {< 0.1} | **0.14 ± 0.03** {0.2 ± 0.1} | 0.03 ± 0.04 | 0.05 ± 0.05 | 180 |
| none | 0.02 ± 0.05 {0.17 ± 0.07} | 0.03 ± 0.03 {0.2 ± 0.2} | <0.03 {<0.2} | 0.04 ± 0.02 | |

[a]lisin = lisinopril. [b]For reactions with initial rates of inactivation (monitored by fluorogenic substrate cleavage) that were above background (shown in bold), initial rates of cleavage of full-length sACE-1 (monitored by SDS−PAGE) are listed for comparison (shown in braces). [c]Reduction potentials of the M−chelate domains were determined previously;[12] redox couples are 3+/2+ for Fe, Co, Ni−ATCUN, and Cu−ATCUN complexes and 2+/1+ for all other Ni and Cu complexes.

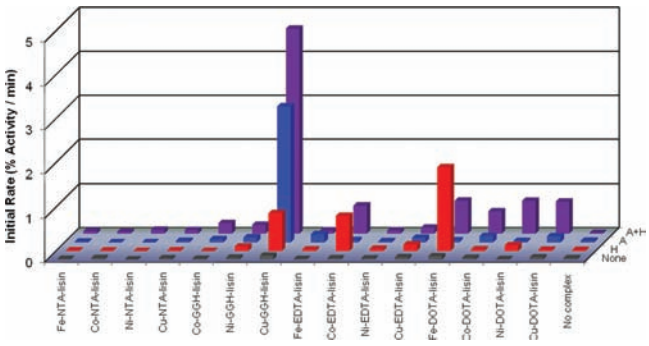


**Figure 5.** Initial rates for inactivation of sACE-1 by M−chelate−lisinopril complexes with the coreactants 1 mM ascorbate and 1 mM $H_2O_2$ (A + H), 1 mM ascorbate (A), and 1 mM $H_2O_2$ (H) or with no coreactant (none).

activity was observed even after several hours of incubation and appeared to be the result of either quantitative conversion of sACE-1 to forms displaying reduced activity, through either modification of amino acid side chains or cleavage of the protein backbone (or both) that diminished, but did not completely abolish, substrate binding and hydrolysis,[15] or in part depletion of redox coreactants, since addition of fresh ascorbate and peroxide resulted in further modest reductions in activity. Following inactivation with each M−chelate−lisinopril complex and coreactants, the substrate cleavage activity of inactivated sACE-1 was monitored using a range of substrate concentrations, and the percentage of full-length sACE-1 remaining was independently quantified by SDS−PAGE with silver staining (Figure SM37 and Table SM6, Supporting Information). The Michaelis−Menten kinetic parameters $k_{cat}$, $K_M$, and $k_{cat}/K_M$ for substrate cleavage by inactivated sACE-1 as well as the percentage of full-length sACE-1 remaining (percentage that was not cleaved) after preincubation are listed in Table 3. The predominant mechanism of sACE-1 inactivation for each catalyst (side chain modification vs protein cleavage) was assessed by comparison of the remaining percentage of $k_{cat}/K_M$ and the percentage of full-length sACE-1 remaining following preincubation. Inactivation of sACE-1 appeared to occur primarily as a result of side chain modification, rather than backbone cleavage, since the observed decrease in full-length sACE-1 remaining was typically not significant enough to account for even half of the larger overall decreases in $k_{cat}/K_M$; this result is consistent with the fact that higher initial rates were observed for inactivation than for cleavage. Additionally, it is possible that certain backbone cleavage events could arise only as a result of initial side chain oxidation. The enzyme efficiency ($k_{cat}/K_M$) of inactivated sACE-1 was observed to decrease by as much as 12-fold (for Cu−GGH−lisinopril) relative to that of unmodified sACE-1, and this decreased enzyme efficiency resulted from an increased $K_M$, a decreased $k_{cat}$, or both, depending on the complex used, and conversion from active to inactivated enzyme required the presence of both M−chelate−lisinopril and coreactants (Figures SM35 and SM36, Supporting Information). The reaction pathway for sACE-1 inactivation appeared to vary depending on the M−chelate−lisinopril complex used. Increased $K_M$ values, which most likely reflect oxidation of sACE-1 residues that contribute to substrate binding by sACE-1, were observed for all complexes except for Co− and Ni−GGH−lisinopril and Ni− and Cu−DOTA−lisinopril, and increases in $K_M$ were highest for M−EDTA−lisinopril, Co−NTA−lisinopril, and Fe−DOTA−lisinopril complexes. Decreases in $k_{cat}$, reflecting either protein cleavage or modification of active site residues directly involved in catalytic hydrolysis of substrate, were observed for all complexes, with the exception of Fe−, Co−, and Ni−NTA−lisinopril and Fe− and Ni−EDTA−lisinopril. The magnitude of the decrease in $k_{cat}$ was greatest for M−GGH−lisinopril, M−DOTA−lisinopril, and Cu−chelate−lisinopril complexes. The relative changes in the $k_{cat}$ and $K_M$ of sACE-1, as well as the relative level of sACE-1


dx.doi.org/10.1021/ja208791f | J. Am. Chem. Soc. 2012, 134, 3396−3410

**Table 3. Characterization of Inactivated sACE-1: Michaelis–Menten Kinetic Parameters for Cleavage of the Substrate Mca-RPPGFSAFK(Dnp)-OH by Inactivated sACE-1 and Percentage of Full-Length sACE-1 Remaining Following Preincubation of sACE-1 with M–Chelate–Lisinopril Complexes and Coreactants**

| | kinetic parameters for substrate cleavage by inactivated sACE-1[b] | | | |
|---|---|---|---|---|
| complex[a] | $k_{cat}$ ($min^{-1}$) | $K_M$ ($\mu M$) | $k_{cat}/K_M$ ($min^{-1}$ $\mu M^{-1}$) | percentage of full-length sACE-1 remaining after incubation[c] |
| Fe–NTA–lisin | 1180 ± 80 | **9 ± 2** | **130 ± 30 (48%)** | 86 ± 2 |
| Co–NTA–lisin | 1500 ± 200 | **13 ± 4** | **110 ± 40 (41%)** | 91 ± 3 |
| Ni–NTA–lisin | 1200 ± 100 | **8 ± 2** | 150 ± 40 (56%) | 96 ± 1 |
| Cu–NTA–lisin | **910 ± 10** | **7.5 ± 0.3** | **122 ± 6 (45%)** | 90 ± 20 |
| Co–GGH–lisin | **750 ± 20** | 4.6 ± 0.5 | 160 ± 20 (59%) | 80 ± 20 |
| Ni–GGH–lisin | **840 ± 30** | 6.3 ± 0.6 | **130 ± 10 (48%)** | **70 ± 20** |
| Cu–GGH–lisin | **150 ± 10** | **7 ± 1** | **22 ± 4 (8.1%)** | **50 ± 40** |
| Fe–EDTA–lisin | 1350 ± 40 | **10.9 ± 0.9** | **120 ± 10 (44%)** | 80 ± 30 |
| Co–EDTA–lisin | **780 ± 10** | **11.8 ± 0.3** | **66 ± 2 (24%)** | 89 ± 7 |
| Ni–EDTA–lisin | 1510 ± 50 | **11 ± 1** | **140 ± 10 (52%)** | 85 ± 1 |
| Cu–EDTA–lisin | **218 ± 3** | **11.1 ± 0.4** | **19.7 ± 0.9 (7.3%)** | **40 ± 30** |
| Fe–DOTA–lisin | **540 ± 20** | **15 ± 1** | **36 ± 4 (13%)** | 87 ± 1 |
| Co–DOTA–lisin | **840 ± 10** | **8.7 ± 0.3** | **97 ± 3 (36%)** | 91 ± 9 |
| Ni–DOTA–lisin | **610 ± 30** | 5.6 ± 0.7 | **110 ± 20 (41%)** | 90 ± 30 |
| Cu–DOTA–lisin | **520 ± 20** | 6.0 ± 0.8 | **90 ± 10 (33%)** | **74 ± 1** |
| none | 1220 ± 50 | 4.5 ± 0.6 | 270 ± 40 (100%) | 100 ± 8 |

[a]lisin = lisinopril. [b]$k_{cat}$ values below background, $K_M$ values above background, and $k_{cat}/K_M$ values below background are shown in bold. The percentage of $k_{cat}/K_M$ remaining after each preincubation, relative to the control, is shown in parentheses to allow comparison with the percentage of full-length sACE-1 remaining. The concentration of each complex used for preincubation corresponded to 20% saturation of sACE-1, and ascorbate and $H_2O_2$ were each present at 1 mM. [c]Monitored by SDS–PAGE.

cleavage, that occurred upon inactivation by each M–chelate–lisinopril complex provide useful information regarding which type of active site residues (substrate binding vs substrate hydrolysis) were modified or, alternatively, the degree to which the backbone of sACE-1 was cleaved. Michaelis–Menten parameters for inactivated sACE-1, after inactivation with each M–chelate–lisinopril complex and coreactants, are summarized in Table 3 and are complementary to the results for time-dependent inactivation of sACE-1.

**Kinetic Stability of M–Chelate Complexes.** Of potential concern was the degree to which the stability of each M–chelate–lisinopril complex was affected by the mandatory presence of $Zn^{2+}$, because sACE-1 is a zinc-dependent enzyme. The ability of $Zn^{2+}$ to exchange with $Fe^{3+}$, $Co^{2+}$, $Ni^{2+}$, and $Cu^{2+}$ for the complexes studied was evaluated by incubating $Zn^{2+}$ and each M–chelate (both present at 100 $\mu$M) at 37 °C. Exchange was monitored by UV/vis spectroscopy by following the change in absorbance at the specified wavelengths (Figure SM40, Supporting Information) for each M–chelate over time. All complexes were effectively stable in the presence of $Zn^{2+}$, although very slow exchange was observed for only Fe–EDTA, Co–EDTA, and Fe–DOTA, with apparent second-order rate constants for exchange of 350 ± 10, 480 ± 20, and 3.1 ± 0.1 $M^{-1}$ $min^{-1}$, respectively (Table SM7, Supporting Information). Although the rates of exchange with $Zn^{2+}$ could not be directly measured at the low concentrations of catalysts used for sACE-1 binding and catalytic inactivation experiments, due to the low absorbance of M–chelates at these concentrations, exchange with $Zn^{2+}$ for all species appeared to be insignificant at these concentrations, based on apparent second-order rate constants. For example, displacement of iron from 1 $\mu$M Fe–EDTA by 10 $\mu$M $Zn^{2+}$ would occur at a calculated initial rate of only $3.5 \times 10^{-9}$ M/min, or 0.35% of the metal complex/min. The fact that both sACE-1 binding and sACE-1 inactivation by Fe–DOTA–, Fe–EDTA–, and Co–EDTA–lisinopril followed expected trends further supports the observation that these complexes were effectively stable under the conditions used.

## DISCUSSION

**Concentration-Dependent Inactivation of sACE-1.** The ability of each M–chelate–lisinopril complex to catalytically inactivate sACE-1 was dependent upon both the sACE-1 binding affinity and the kinetics of irreversible sACE-1 inactivation by M–chelate–lisinopril complexes following active site binding. Prior to the kinetics of irreversible sACE-1 inactivation by the M–chelate–lisinopril complexes being studied, the relative affinities of each M–chelate–lisinopril complex for sACE-1 were determined. Each M–chelate–lisinopril complex was tested for the ability to reversibly inhibit sACE-1 activity, and for each M–chelate–lisinopril species the concentration dependence was expressed as the half-maximal inhibitory concentration ($IC_{50}$). The sACE-1 binding affinities of M–chelate–lisinopril species were greatly enhanced relative to those of the respective M–chelates lacking lisinopril, as expected, and the sACE-1 binding affinities of the M–chelate–lisinopril species were found to be inversely correlated with both the size and negative charge of the attached M–chelates (Figure 6), whereas the degree of coordination unsaturation of the attached M–chelate appeared to variably affect the sACE-1 binding affinity.

Attachment of smaller M–chelates to lisinopril, as in the case of M–NTA–lisinopril, resulted in tighter binding to the active sites of sACE-1 (lower $IC_{50}$ values), whereas increases in the size of the attached M–chelate (M–NTA < M–GGH < M–EDTA < M–DOTA) incrementally reduced the binding affinity for sACE-1. The M–DOTA–lisinopril complexes, which contain the largest M–chelates, had the weakest ACE affinity among the M–chelate–lisinopril complexes tested. Structural modeling confirmed this correlation, since lisinopril-attached M–DOTA had difficulty entering the active site of both N-domain ACE and C-domain ACE during energy


dx.doi.org/10.1021/ja208791f | J. Am. Chem. Soc. 2012, 134, 3396–3410

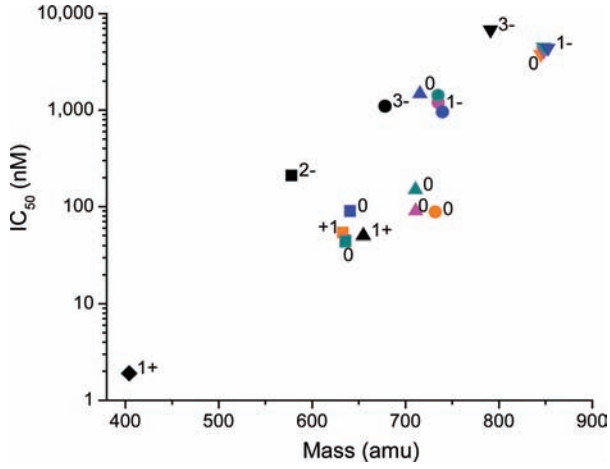


**Figure 6.** sACE-1 binding affinity of M−chelate−lisinopril complexes was inversely correlated with the size and negative charge of the species attached to the lysine side chain of lisinopril. Lisinopril and all M−chelate−lisinopril species (metal-bound and metal-free) are shown: ◆, lisinopril; ■, NTA−lisinopril; ▲, GGH−lisinopril; ●, EDTA−lisinopril; ▼, DOTA−lisinopril; orange, Fe; pink, Co; cyan, Ni; blue, Cu; black, no metal. The charge of the modified lysine side chain of lisinopril is listed for each attachment; the charge for each $Fe^{3+}$ complex was 1+ higher than for each corresponding $M^{2+}$ complex.

minimization, whereas lisinopril-attached M−NTA, M−GGH, and M−EDTA all preferred localization within the active site binding pockets of ACE. Additionally, the planar profile of the attached M−chelate appeared to contribute to ACE affinity. M−GGH−lisinopril complexes that contain relatively low profile square-planar M−GGH chelates tended to have lower $IC_{50}$ values. The sole exception was Cu−GGH−lisinopril, possibly reflecting a distinct structure compared to other M−GGH−lisinopril complexes in the unbound state as a result of intramolecular coordination of one of the two lisinopril carboxylates to an axial coordination site of the Cu−GGH−lisinopril complex. Indeed, the square-planar Cu−GGH complex is known to weakly coordinate a fifth oxygen ligand at one of the two axial coordination sites, probably as a result of Jahn−Teller distortion of the $d^9$ $Cu^{2+}$ center,[33] and energy-minimized 3D models of Cu−GGH−lisinopril are consistent with the required geometry. Cu−GGH−lisinopril could alternatively accommodate intermolecular axial coordination to a nearby amino acid side chain from sACE-1, such as D140 from the N-terminal domain or E162 or D377 from the C-terminal domain, although this is less likely, as evidenced by the higher $IC_{50}$ value. The M−NTA−lisinopril complexes similarly possess two empty metal-coordination sites, which also have the potential for either intramolecular coordination to lisinopril carboxylates or intermolecular coordination to sACE-1 amino acid side chains. The latter most likely contributes to the observed high-affinity binding to sACE-1 by the M−NTA−lisinopril complexes. M−NTA−lisinopril complexes differ from Cu−GGH−lisinopril in that the empty metal-coordination sites of M−NTA−lisinopril appear to favor sACE-1 binding through coordination of sACE-1 residues, whereas sACE-1 binding appears to be abrogated by empty coordination sites in the case of Cu−GGH−lisinopril, most likely through distinct modes of intermolecular and intramolecular metal coordination, respectively. Another key difference between the metal-coordination environments of M−NTA− and M−GGH−lisinopril is that the two empty coordination sites of each exist in *cis* and *trans* orientations, respectively, and this difference could partially contribute to their distinct binding affinities for sACE-1.

In addition to steric and metal-coordination effects, the charge of the M−chelates attached to lisinopril appeared to affect the affinity of the M−chelate−lisinopril complexes toward sACE-1. The charge ($z$) of the M−chelates coupled to the lysine side chain of lisinopril increased from negative to positive in the order M−DOTA = M−EDTA ($z = -1$) < M−GGH = M−NTA ($z = 0$) < uncoupled amine ($z = +1$) for noniron complexes, and the observed sACE-1 binding affinity followed the same trend. Metal-bound chelators typically had a more positive charge than metal-free chelators (except for GGH−lisinopril) as a result of the positive charge of the bound metal, and these followed the same trend. Similarly, iron complexes of EDTA−lisinopril and DOTA−lisinopril were observed to possess significantly higher sACE-1 binding affinity than the analogous complexes with cobalt, nickel, and copper as a result of the greater 3+ oxidation state relative to those of the other metals. Indeed, X-ray crystal structures of the lisinopril/ACE complex show a close proximity between the negatively charged ACE residues (D140 for N-domain ACE; D377 and E162 for tACE) and the positively charged lysine side chain of ACE-bound lisinopril,[5,6] and the resulting electrostatic attraction most likely contributes to the high-affinity binding of sACE-1 by lisinopril. Conversion of the positively charged lysine side chain of lisinopril to a negative or neutral M−chelate is expected to negatively impact the sACE-1 binding affinity to some degree, as is observed. Lisinopril had the highest affinity for sACE-1 ($IC_{50}$ = 1.9 nM) of all species studied, which punctuates the inverse correlations between sACE-1 binding affinity and both size and negative charge of attached M−chelates. However, the binding interaction between lisinopril and sACE-1 was sufficiently tolerant of attachment of M−chelates to lisinopril that high-affinity binding was retained for each of the M−chelate−lisinopril species, and this high-affinity binding is a prerequisite for targeted catalytic inactivation of sACE-1 by M−chelate−lisinopril complexes.

**Domain Selectivity.** A possible consequence of attachment of M−chelates to lisinopril is that the modest selectivity of lisinopril for the C-domain of sACE-1, which is thought to result from the higher negative charge density within the C-domain active site that lies in close proximity to the lysine side chain of lisinopril,[6] could become reversed, so that binding to the N-domain is more favored. Keeping in mind that previous studies have demonstrated the N-domain to be a slightly more efficient catalyst of angiotensin I hydrolysis than the C-domain ($k_{cat}/K_M$ = 13 $\mu M^{-1}$ $min^{-1}$ for the N-domain vs 9.6 $\mu M^{-1}$ $min^{-1}$ for the C-domain and 11 $\mu M^{-1}$ $min^{-1}$ for sACE-1), despite similar substrate binding affinities ($K_M$ values ranging from approximately 17 to 19 $\mu M$),[37] and that there is much evidence for unique critical roles of the N-domain in hematopoietic stem cell regulation,[38] the inversion of inhibitor selectivity in favor of binding to the N-domain could be beneficial for certain therapeutic uses. The inverse correlation between negative charge and binding affinity most likely applies to both active sites. However, our experiments with somatic ACE-1 and the substrate Mca-RPPGFSAFK(Dnp)-OH, which is derived from bradykinin (RPPGFSPFR), a C-domain-selective substrate,[39] most likely reflect binding/inactivation of the C-domain and therefore provide no assessment of domain selectivity. Consistent with this fact, reported $k_{cat}/K_M$ values for hydrolysis of a fluorogenic substrate similar to that used herein (Abz-LFK(Dnp)-OH) by N-domain ACE, tACE


dx.doi.org/10.1021/ja208791f | J. Am. Chem. Soc. 2012, 134, 3396−3410

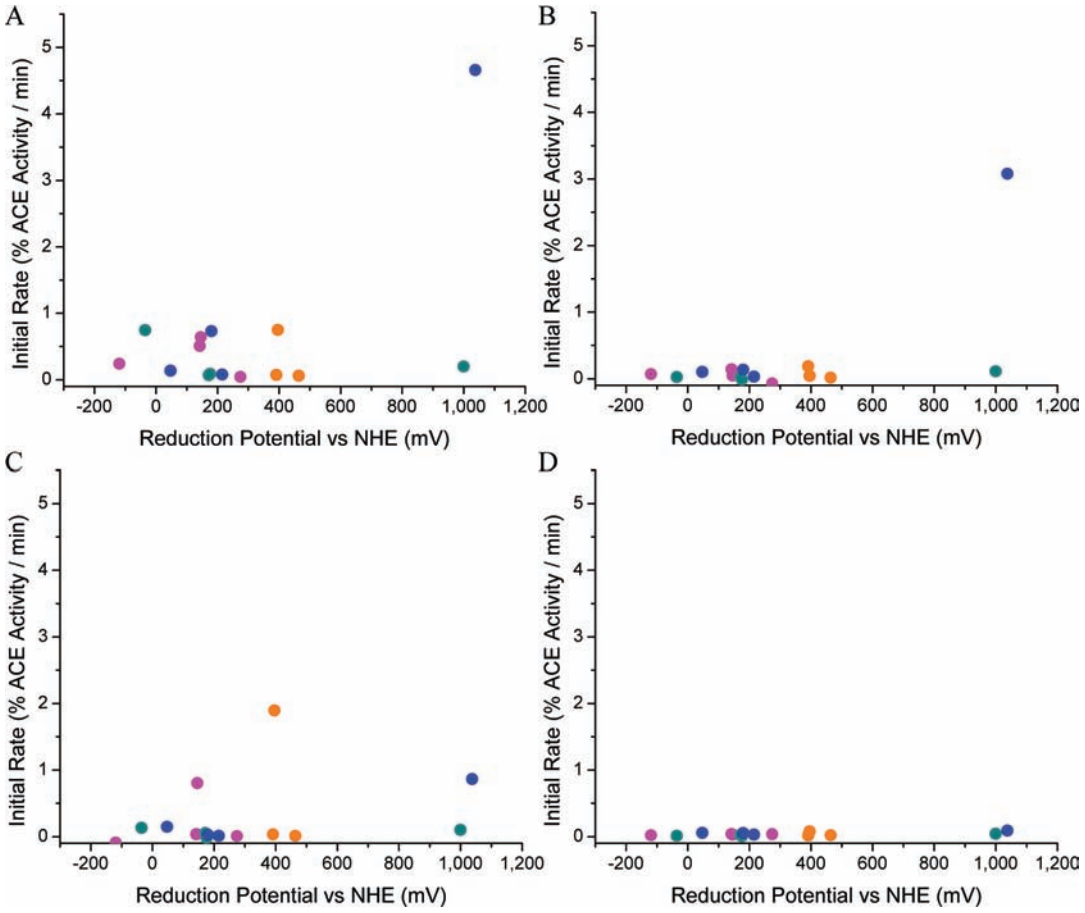


**Figure 7.** Initial rates of aerobic sACE-1 inactivation by M−chelate−lisinopril complexes and added coreactants: (A) $H_2O_2$/ascorbate, (B) ascorbate, (C) $H_2O_2$, (D) none; orange, Fe; pink, Co; cyan, Ni; blue, Cu. Rates depended on the coreactants present and were highest for M−chelates with reduction potentials near 1000 mV (high region), and modest rates were seen for reduction potentials (low potential region) between those of $H_2O_2$/hydroxyl radical ($E^\circ$ = +380 mV) and ascorbyl radical/ascorbate ($E^\circ$ = −66 mV). Rates of catalysis were negligible in the absence of added coreactant.

(identical to the C-domain), and sACE-1 are 10 $\mu M^{-1}$ $min^{-1}$ ($k_{cat}$ = 60 $min^{-1}$), 380 $\mu M^{-1}$ $min^{-1}$ ($k_{cat}$ = 1240 $min^{-1}$), and 220 $\mu M^{-1}$ $min^{-1}$ ($k_{cat}$ = 798 $min^{-1}$), respectively,[40] although the exact domain selectivity of the substrate Mca-RPPGFSAFK-(Dnp)-OH is unknown. Clarification of the domain selectivity of the M−chelate−lisinopril complexes will be the focus of future studies.

**Kinetics and Mechanism of Catalytic Inactivation.** Catalytic inactivation of sACE-1 was observed for most of the M−chelate−lisinopril complexes investigated in this work, and these complexes provided a remarkable range of reactivity. Catalytic inactivation of sACE-1 by M−chelate−lisinopril complexes was found to be dependent upon the ability of lisinopril to localize each attached M−chelate to the active sites of sACE-1 and the specific properties of each M−chelate, including the reduction potential, coordination environment, and identity of the transition metal present within each M−chelate. M−chelate−lisinopril reactivity was amplified by the presence of physiologically available redox coreactants, which provided the driving force responsible for the observed reactivity. The presence/absence of the coreactants ascorbate and $H_2O_2$, which have reported physiological concentrations ranging from micromolar to millimolar and from picomolar to micromolar, respectively, were varied to evaluate the redox mechanism and coreactant selectivity.[41,42] We believe the catalytic reaction to be similar for ascorbate/$O_2$ and ascorbate/peroxide systems, with the introduction of peroxide providing a mechanistic "shunt", with cytochrome P450 providing good precedent for formation of peroxide at a catalytic redox center from $O_2$ and an electron source.[43]

The ability of each M−chelate−lisinopril complex to catalyze irreversible inactivation of sACE-1 was attributed to the known ability of M−chelates to facilitate conversion of the oxidant $O_2$ or $H_2O_2$ to reactive oxygen species (ROS) through single-electron transfer,[44−46] followed by the reaction of nascent ROS with nearby sACE-1 residues, resulting in active site destruction. Meanwhile, ascorbate, a single-electron reductant, is known to function as a pro-oxidant by rereducing oxidized metal centers following generation of ROS.[46−48] Therefore, in the presence of both oxidant and reductant, M−chelate complexes possess the ability to undergo multiple turnovers of oxidation/reduction, catalyzing production of multiple ROS per metal center in the process (Figures SM41−SM43, Supporting Information). This ability of M−chelates to function with multiple turnovers was previously observed to be optimal when the M−chelate reduction potential is poised between the reduction potentials of the reductant and oxidant half-reactions, since both reduction and oxidation of the M−chelate are thermodynamically favored in this range; a similar theme is employed by native superoxide dismutase (SOD), in which the reduction potential of SOD is poised between those of the two relevant half-reactions.[49,50] The reduction potentials

for ascorbyl radical/ascorbate and $H_2O_2/OH^•$ at neutral pH are −66 and 380 mV,[51,52] respectively, and we demonstrated previously that M−chelates with reduction potentials within this range provide the fastest rates of consumption of redox coreactants, ROS generation, and multiple-turnover redox cycling of the M−chelate. As a result, M−chelate-mediated cleavage of both DNA and RNA was observed to be optimal within this range, while reduction potentials outside this range provided very mild levels of reactivity.[12,26] However, a key difference between nucleic acid and protein targets, such as sACE-1, is that proteins tend to be more stable than nucleic acids toward oxidative insults.[36,53] Therefore, nucleic acid cleavage by M−chelates appears to be optimized by selection of M−chelates with reduction potentials that lie close to those of relevant coreactants, with facile subsequent cleavage of nucleic acids by nascent ROS. By contrast, the efficiency of enzyme inactivation by M−chelates is more likely to require optimization of catalyst reduction potentials to match specific amino acid and/or protein backbone oxidation requirements, which are more demanding than for nucleic acids. For example, previously determined reduction potentials for $Tyr^{•+}$/Tyr, $Trp^{•+}$/Trp, and $His^{•+}$/His at pH 7 are 930, 1015, and 1170 mV, respectively,[36,53] and these residues each exist within the active sites of sACE-1.[5,6] Indeed the fastest rates of sACE-1 inactivation were observed for Cu−GGH−lisinopril, and the Cu−GGH chelate displays the highest reduction potential of the M−chelates tested, $E°$ = 1038 mV. Accordingly, inactivation of sACE-1 appears to be mediated by oxidation of active site residues and, to a lesser extent, cleavage of the protein backbone (Table 2), consistent with our previous observations for metallopeptide-mediated inactivation of human carbonic anhydrase,[15] as well as the reduced catalytic efficiency of inactivated sACE-1.

Two hot spots were observed in the relationship between the rate of sACE-1 inactivation and the M−chelate reduction potential, namely, a low potential region and a high potential region (Figure 7). The low potential region, which ranged from approximately −100 to +400 mV, provided relatively mild levels of sACE-1 inactivation, and M−chelate reactivity in this range was attributed to the redox cycling described above, where $H_2O_2$ is converted to hydroxyl radicals and ascorbate rereduces the oxidized metal center, allowing thermodynamically favored multiple turnovers and ROS generation. Indeed activity in this range was highest when both $H_2O_2$ and ascorbate were present. The high potential region, which corresponded to M−chelate reduction potentials near 1000 mV, provided the most efficient catalytic inactivation of sACE-1. M−chelates in this range (Cu−GGH and Ni−GGH) have greater oxidizing power, although prerequisite generation of the oxidized metal is less thermodynamically favored and probably requires an alternate mechanism. The most likely mechanism involves (1) metal-mediated reduction of $O_2$ by ascorbate to form metal-bound superoxide, (2) single-electron oxidation of the reduced metal center by metal-bound superoxide, forming $H_2O_2$ (possibly metal-bound) with the possibility of subsequent Fenton chemistry, resulting in a metal-associated reactive oxygen species, and (3) reaction of this activated species with nearby sACE-1 residues, resulting in sACE-1 inactivation. Each step of this mechanism is supported, respectively, by the facts that (1) Ni−GGH−lisinopril and Cu−GGH−lisinopril are reactive in the presence of the combination of $O_2$ and ascorbate, the addition of $H_2O_2$ further stimulates reactivity (mechanistic shunt), and the lack of diffusion of superoxide radicals in our previous work suggests that the superoxide intermediate is metal-bound (Figure SM42, Supporting Information),[26] (2) the reduction potential of the superoxide/$H_2O_2$ half-reaction ($E°$ = 890 mV) lies closest to 1000 mV of any of the possible single-electron half-reactions between $O_2$, superoxide, $H_2O_2$, and hydroxyl radical,[51] and superoxide is therefore the most likely species to oxidize the metal center, and (3) these M−chelate−lisinopril complexes catalyzed irreversible inactivation of sACE-1 with high efficiency. Interestingly, in our previous work on M−chelate-promoted nucleic acid cleavage we observed that activity was centered in the same two regions (low and high potential range of $E°$), although nucleic acid cleavage was significantly faster for the low potential region than for the high potential region. This pattern now appears to be inverted in the case of protein (sACE-1) inactivation and most likely reflects the different chemical makeups of the targets (protein vs nucleic acid) and relative difficulty of oxidation of protein side chains and/or backbone versus (deoxy)ribose rings.

The coreactant dependence of the catalytic activity of each M−chelate−lisinopril species appeared to be related to the reduction potential, coordination environment, and electronic properties of each attached M−chelate. For instance, Cu−GGH−lisinopril and Ni−GGH−lisinopril each possess reduction potentials near 1000 mV. However, observed reactivity was much higher for Cu−GGH−lisinopril than for Ni−GGH−lisinopril. Several factors could contribute to the enhanced reactivity of the copper site. In particular, the $d^9$ configuration of $Cu^{2+}$ is subject to the Jahn−Teller effect that will labilize the nonchelating axial sites and facilitate coreactant and reactant binding and product release, whereas $Ni^{2+}$ is a relatively stable square-planar $d^8$ system. Also, oxidation of $Cu^{2+}$ yields the electronically stable square-planar $d^8$ $Cu^{3+}$ center, relative to $Ni^{2+}$ oxidation where it is lost, so the former reaction is expected to have lower activation barrier and be kinetically favored. Similarly, the iron complexes Fe−DOTA−lisinopril, Fe−EDTA−lisinopril, and Fe−NTA−lisinopril each possess reduction potentials near 400 mV, but show different coreactant selectivities. Fe−DOTA−lisinopril (and Co−EDTA−lisinopril) preferred reaction with the co-oxidant $H_2O_2$, with no obvious enhancement following addition of ascorbate, whereas Fe−EDTA−lisinopril preferred reaction with $O_2$ and ascorbate; Fe−NTA−lisinopril surprisingly had no apparent reactivity.[45] We have previously observed that both Fe−DOTA and Co−EDTA produce hydroxyl radicals in the presence of $H_2O_2$, but not $O_2$ (Figure SM42, Supporting Information), and that these complexes do not readily consume ascorbate (Figure SM41, Supporting Information), consistent with the lack of enhancement of catalytic activity with added ascorbate for these two complexes.[26] We also previously observed that Fe−EDTA reacts with either $O_2$/ascorbate or $H_2O_2$/ascorbate to efficiently produce superoxide radicals or hydroxyl radicals, respectively (Figure SM42).[26] The fact that inactivation of sACE-1 by Fe−EDTA−lisinopril was more dependent on $O_2$ than $H_2O_2$ suggests that superoxide radicals more effectively inactivated sACE-1 than hydroxyl radicals. It was surprising that no catalytic activity was observed for Fe−NTA−lisinopril, since Fe−NTA was also previously found to react rapidly with both $H_2O_2$/ascorbate and $O_2$/ascorbate to produce ROS, so the lack of reactivity of M−NTA−lisinopril complexes in general may reflect the fact that the two *cis* empty coordination sites of M−NTA−lisinopril are actually occupied by an active site sACE-1 residue, blocking reaction with


dx.doi.org/10.1021/ja208791f | J. Am. Chem. Soc. 2012, 134, 3396−3410

**Table 4. Second-Order Rate Constants for Both Inactivation and Cleavage of Full-Length sACE-1 by Several M−Chelate−Lisinopril Complexes and Control Experiment Second-Order Rate Constants for the Corresponding M−Chelates Lacking Lisinopril**

| | $k_2$ for inactivation {and cleavage} of full-length sACE-1 ($M^{-1}$ $min^{-1}$)[b] | | |
|---|---|---|---|
| complex[a] | M−chelate−lisinopril | without lisinopril | conditions[c] |
| Cu−GGH−lisin | 152000 ± 7000 {70000 ± 20000} | 10000 ± 5000 {<3000} | ascorbate + $H_2O_2$ |
| Fe−EDTA−lisin | 110000 ± 30000 {<100000} | 10000 ± 50000 {<100000} | ascorbate |
| Cu−GGH−lisin | 102000 ± 6000 {<6000} | <1000 {*d*} | ascorbate |
| Co−GGH−lisin | 70000 ± 40000 {<70000} | <20000 {*d*} | ascorbate + $H_2O_2$ |
| Co−EDTA−lisin | 40000 ± 10000 {10000 ± 7000} | <4000 {*d*} | $H_2O_2$ |
| Co−EDTA−lisin | 30000 ± 10000 {< 3000} | <3000 {*d*} | ascorbate + $H_2O_2$ |
| Ni−GGH−lisin | 30000 ± 20000 {<60000} | <5000 {*d*} | ascorbate |
| Cu−GGH−lisin | 28000 ± 9000 {15000 ± 6000} | <2000 {*d*} | $H_2O_2$ |
| Fe−DOTA−lisin | 22000 ± 5000 {<2000} | <600 {*d*} | $H_2O_2$ |
| Fe−DOTA−lisin | 8000 ± 1000 {3000 ± 1000} | <400 {*d*} | ascorbate + $H_2O_2$ |
| Ni−DOTA−lisin | 7000 ± 1000 {<600} | <700 {*d*} | ascorbate + $H_2O_2$ |
| Cu−DOTA−lisin | 6200 ± 900 {<1000} | <500 {*d*} | ascorbate + $H_2O_2$ |
| Cu−EDTA−lisin | 5000 ± 4000 {<9000} | <3000 {*d*} | $H_2O_2$ |
| Co−DOTA−lisin | 5000 ± 1000 {2000 ± 2000} | <700 {*d*} | ascorbate + $H_2O_2$ |
| Cu−EDTA−lisin | 3000 ± 2000 {2000 ± 9000} | 2000 ± 3000 {*d*} | ascorbate |
| Cu−DOTA−lisin | 1000 ± 400 {<2000} | <1000 {*d*} | ascorbate |

[a]lisin = lisinopril. [b]Second-order rate constants for inactivation of sACE-1 (measured by substrate cleavage) and for cleavage of full-length sACE-1 (monitored by SDS−PAGE) are listed for comparison (cleavage data shown in braces). [c]All experiments throughout this study were performed at pH 7.4 and 37 °C. [d]Not determined.

coreactants,[44] consistent with the observed high-affinity binding of sACE-1 by the M−NTA−lisinopril species.

The nature of the ROS produced by each M−chelate−lisinopril complex (superoxide, $H_2O_2$, or hydroxyl radical) and whether the ROS was metal-bound or diffusible were likely to be key factors in determining the catalytic efficiency of sACE-1 inactivation for each M−chelate−lisinopril complex, since the most critical contribution to catalysis, other than binding affinity, appears to be the step in which ROS or ROS-activated M−chelates react directly with active site sACE-1 residues. Our data show no correlation between reactivity and the rate of production of diffusible hydroxyl radical or superoxide species, as reflected by rates of ascorbate consumption (Figure SM41, Supporting Information) or reaction with 4-((9-acridinecarbonyl)amino)-2,2,6,6-tetramethylpiperidin-1-oxyl, free radical (TEMPO-9-Ac) and rhodamine B radical traps (Figures SM42 and SM43, Supporting Information).[26] Cu−GGH−lisinopril, the most effective catalyst, appears most likely to inactivate sACE-1 through an activated metal-bound ROS intermediate, rather than through the production of diffusible radicals, so the most effective M−chelate−lisinopril intermediates were likely to be metal-bound ROS, since a metal-bound ROS would be held in close proximity to the active site for an extended period of time. Similarly, the complexes Ni−GGH, Co−GGH, Co−DOTA, Ni−DOTA, and Cu−DOTA were each found to effectively inactivate sACE-1, but none of these complexes were found to produce diffusible radicals in our previous studies (Figures SM42 and SM43).[26] Even for complexes known to produce diffusible radicals, such as Fe−EDTA, Fe−NTA, Fe−DOTA, and Co−EDTA, the ROS produced are likely to remain bound to the metals where they originated for a significant period of time before diffusing, and this metal-bound state is most likely responsible for most of the observed catalytic inactivation of sACE-1 for Fe−EDTA−, Fe−DOTA−, and Co−EDTA−lisinopril. We have also observed this proximity effect in previous studies involving targeted cleavage of HIV Rev response element (RRE) RNA by Rev-coupled M−chelates, in which the most effective M−chelates were those not observed to produce diffusible radicals.[12] Those M−chelate−lisinopril complexes, such as Cu−GGH−lisinopril, that are effective catalysts but do not produce a damaging abundance of diffusible ROS are likely to possess the best characteristics for physiological use due to their selective nature of targeted catalytic inactivation. In fact, the in vivo abundance of native ATCUN motifs, such as GGH, in albumins,[33,34,54,55] histatins,[56,57] and neuromedin C,[58] typically used for Cu- and Ni-transport, as well as selective oxidation chemistry, most likely reflects both the placement of the Cu−ATCUN and Ni−ATCUN reduction potentials outside of the typical physiological window and the lack of diffusible ROS produced by these complexes. In this study, we have effectively hijacked the natural Cu−ATCUN complex for the purpose of targeted inactivation of sACE-1.

To elucidate the overall catalytic efficiencies of irreversible sACE-1 inactivation and cleavage by the synthesized M−chelate−lisinopril complexes, second-order rate constants were established by use of eq 2 and are summarized in Table 4. M−chelate−lisinopril complexes were found to inactivate sACE-1 with a remarkable range of second-order rate constants, as high as 150 000 $M^{-1}min^{-1}$, and many were able to do so under physiologically relevant conditions. Attachment to lisinopril was necessary for targeted inactivation of sACE-1 by M−chelate−lisinopril complexes, as evidenced by the large increase in second-order rate constants for inactivation of sACE-1 upon attachment of M−chelates to lisinopril. The magnitude of each second-order rate constant was dependent primarily on the relative ability of each M−chelate−lisinopril catalyst to both bind sACE-1 with high affinity and irreversibly modify active site residues of sACE-1 following binding.

## ■ CONCLUSIONS

Catalytic metallodrugs possess the potential for highly efficient multiple-turnover, irreversible inactivation of therapeutic targets. Here we have demonstrated that, through attachment


dx.doi.org/10.1021/ja208791f | J. Am. Chem. Soc. 2012, 134, 3396−3410

of a variety of reactive metal chelates to a targeting ligand (lisinopril), a remarkable range of catalytic activities toward a targeted enzyme (sACE-1) can be achieved and, furthermore, that it is possible to tune this reactivity to physiological optima by varying parameters of the attached metal complex, including size, charge, coreactant selectivity, coordination environment, and reduction potential. We have illustrated that the size and charge of the attached metal complex greatly affect the relative ability of each catalyst to bind sACE-1 with high affinity and, therefore, to efficiently catalyze inactivation of sACE-1, and these results are likely to prove useful in further development of ACE inhibitors, while similar trends are likely to apply in the development of metallodrugs for other targets. We found that catalytic sACE-1 inactivation was most effective when the catalyst reduction potential was near 1000 mV, in contrast to previous studies of nucleic acid cleavage, where highest activity was observed when the catalyst reduction potential was poised between those of the milder physiological coreactants;[12,26] the relative extremity of the catalyst reduction potential favored for sACE-1 inactivation most likely reflects the increased stability of enzymes relative to nucleic acids toward oxidation and the increased oxidative power required to modify most amino acids. The ability of each catalyst to inactivate sACE-1 appeared to depend to a great extent upon the mechanism employed, and catalysts that inactivated sACE-1 by a metal-bound ROS appeared to function more efficiently than those known to produce diffusible ROS. Catalysts that proceed through metal-bound, rather than diffusible, ROS are likely to prove more valuable for physiological use, since diffusible ROS would be hazardous to nontargeted tissues. This class of compounds possesses a significant advantage over the current reversible inhibitor lisinopril, in that irreversible inactivation of sACE-1 is achieved, and this work marks significant progress toward the ultimate goal of the design of highly efficient multiple-turnover metallodrugs.

## ■ ASSOCIATED CONTENT

### Supporting Information

HPLC traces, mass spectra, $^1$H NMR spectra, metal ion titrations, and extinction coefficients for synthesized M−chelate−lisinopril complexes, concentration-dependent sACE-1 inhibition plots, time-dependent sACE-1 inactivation and cleavage plots, additional rate constants and rates, complex kinetic stability, energy-minimized structural models of M−chelate−lisinopril complexes bound to N-domain ACE, Michaelis−Menten plots and SDS−PAGE analyses for inactivated sACE-1, and redox reactivity of M−chelates. This material is available free of charge via the Internet at http://pubs.acs.org.

## ■ AUTHOR INFORMATION

### Corresponding Author

cowan@chemistry.ohio-state.edu

## ■ ACKNOWLEDGMENTS

This work was supported by grants from the National Institutes of Health (HL093446 and AA016712). J.C.J. was supported by an NIH Chemistry/Biology Interface training grant (T32 GM08512). L.H. was supported by a fellowship from the Ministry of Science and Technology, Thailand. Dr. Michael Freitas kindly allowed use of his LCQ-Deca mass spectrometer, and the Bruker MicroTOF instrument used for all other mass analysis was provided by a grant from the Ohio BioProducts Innovation Center. We thank Jingwei Li for his kind assistance with NMR collection and analysis.

## ■ REFERENCES

(1) Brown, N. J.; Vaughan, D. E. *Circulation* **1998**, *97*, 1411−1420.
(2) Deddish, P. A.; Marcic, B.; Jackman, H. L.; Wang, H.-Z.; Skidgel, R. A.; Erdös, E. G. *Hypertension* **1998**, *31*, 912−917.
(3) Chappell, M. C.; Pirro, N. T.; Sykes, A.; Ferrario, C. M. *Hypertension* **1998**, *31*, 362−367.
(4) Georgiadis, D.; Beau, F.; Czarny, B.; Cotton, J.; Yiotakis, A.; Dive, V. *Circ. Res.* **2003**, *93*, 148−154.
(5) Natesh, R.; Schwager, S. L. U.; Sturrock, E. D.; Acharya, K. R. *Nature* **2003**, *421*, 551−554.
(6) Corradi, H. R.; Schwager, S. L. U.; Nchinda, A. T.; Sturrock, E. D.; Acharya, K. R. *J. Mol. Biol.* **2006**, *357*, 964−974.
(7) Deddish, P. A.; Wang, J.; Michel, B.; Morris, P. w.; Davidson, N. O.; Skidgel, R. A.; Erdos, E. G. *Proc. Natl. Acad. Sci. U.S.A.* **1994**, *91*, 7807−7811.
(8) Lonn, E. M.; Yusuf, S.; Jha, P.; Montague, T. J.; Teo, K. K.; Benedict, C. R.; Pitt, B. *Circulation* **1994**, *90*, 2056−2069.
(9) Hocharoen, L.; Cowan, J. A. *Chem.—Eur. J.* **2009**, *15*, 8670−8676.
(10) Cowan, J. A. *Pure Appl. Chem.* **2008**, *80*, 1799−1810.
(11) Jin, Y.; Cowan, J. A. *J. Am. Chem. Soc.* **2006**, *128*, 410−411.
(12) Joyner, J. C.; Cowan, J. A. *J. Am. Chem. Soc.* **2011**, *133*, 9912−9922.
(13) Gokhale, N. H.; Cowan, J. A. *J. Biol. Inorg. Chem.* **2006**, *11*, 937−947.
(14) Jin, Y.; Cowan, J. A. *J. Biol. Inorg. Chem.* **2007**, *12*, 637−644.
(15) Gokhale, N. H.; Bradford, S.; Cowan, J. A. *J. Am. Chem. Soc.* **2008**, *130*, 2388−2389.
(16) Lee, J.; Udugamasooriya, D. G.; Lim, H.-S.; Kodadek, T. *Nat. Chem. Biol.* **2010**, *6*, 258−260.
(17) Gallagher, J.; Zelenko, O.; Walts, A. D.; Sigman, D. S. *Biochemistry* **1998**, *37*, 2096−2104.
(18) Suh, J.; Yoo, S. H.; Kim, G.; Chae, P. S.; Lee, T. Y.; Lee, J.; Lee, J.; Jang, Y. A.; Ko, E. H. *Angew. Chem.* **2007**, *119*, 7194−7197.
(19) Kim, M. G.; Kim, M.-s.; Lee, S. D.; Suh, J. *J. Biol. Inorg. Chem.* **2006**, *11*, 867−875.
(20) Suh, J.; Chei, W. S. *Curr. Opin. Chem. Biol.* **2008**, *12*, 207−213.
(21) Jeong, K.; Chung, W. Y.; Kye, Y.-S.; Kim, D. *Bioorg. Med. Chem.* **2010**, *18*, 2598−2601.
(22) Chei, W. S.; Ju, H.; Suh, J. *J. Biol. Inorg. Chem.* **2011**, *16*, 511−519.
(23) Suh, J.; Chei, W. S.; Lee, T. Y.; Kim, M. G.; Yoo, S. H.; Jeong, K.; Ahn, J. Y. *J. Biol. Inorg. Chem.* **2008**, *13*, 693−701.
(24) Meggers, E. *Chem. Commun.* **2009**, 1001−1010.
(25) Brown, K. C.; Yang, S.-H.; Kodadek, T. *Biochemistry* **1995**, *34*, 4733−4739.
(26) Joyner, J. C.; Reichfield, J.; Cowan, J. A. *J. Am. Chem. Soc.* **2011**, *133*, 15613−15626.
(27) Palmier, M. O.; Van Doren, S. R. *Anal. Biochem.* **2007**, *371*, 43−51.
(28) Mittal, R. R.; Harris, L.; McKinnon, R. A.; Sorich, M. J. *J. Chem. Inf. Model.* **2009**, *49*, 704−709.
(29) Bernstein, K. E.; Welsh, S. L.; Inman, J. K. *Biochem. Biophys. Res. Commun.* **1990**, *167*, 310−316.
(30) Riordan, J. F.; Harper, J. W.; Martin, M. *J. Cardiovasc. Pharmacol.* **1986**, *8* (Suppl. 10), S29−S34.
(31) Ehlers, M. R. W.; Riordan, J. F. *Biochemistry* **1991**, *30*, 7118−7126.
(32) Lu, J.; Stewart, A. J.; Sadler, P. J.; Pinheiro, T. J. T.; Blindauer, C. A. *Biochem. Soc. Trans.* **2008**, *36*, 1317−1321.
(33) Camerman, N.; Camerman, A.; Sarkar, B. *Can. J. Chem.* **1976**, *54*, 1309−1316.
(34) Lau, S.-J.; Kruck, T. P. A; Sarkar, B. *J. Biol. Chem.* **1974**, *249*, 5878−5884.

(35) Stadtman, E. R. *Annu. Rev. Biochem.* **1993**, *62*, 797−821.
(36) Harriman, A. *J. Phys. Chem.* **1987**, *91*, 6102−6104.
(37) Rice, G. I.; Thomas, D. A.; Grant, P. J.; Turner, A. J.; Hooper, N. M. *Biochem. J.* **2004**, *383*, 45−51.
(38) Michaud, A.; Williams, T. A.; Chauvet, M. T.; Corvol, P. *Mol. Pharmacol.* **1997**, *51*, 1070−1076.
(39) Jaspard, E.; Wei, L.; Alhenc-Gelas, F. *J. Biol. Chem.* **1993**, *268*, 9496−9503.
(40) Woodman, Z. L.; Schwager, S. L. U.; Redelinghuys, P.; Carmona, A. K.; Ehlers, M. R. W.; Sturrock, E. D. *Biochem. J.* **2005**, *389*, 739−744.
(41) Sherman, D. L.; Keaney, J. F. Jr.; Biegelsen, E. S.; Duffy, S. J.; Coffman, J. D.; Vita, J. A. *Hypertension* **2000**, *35*, 936−941.
(42) Gokce, N.; Keaney, J. F. Jr.; Frei, B.; Holbrook, M.; Olesiak, M.; Zachariah, B. J.; Leeuwenburgh, C.; Heinecke, J. W.; Vita, J. A. *Circulation* **1999**, *99*, 3234−3240.
(43) Cowan, J. A. *Inorganic Biochemistry. An Introduction*, 2nd ed.; Wiley-VCH: New York, 1997; pp 333−337.
(44) Graf, E.; Mahoney, J.; Bryant, R.; Eaton, J. *J. Biol. Chem.* **1984**, *259*, 3620−3624.
(45) Inoue, S.; Kawanishi, S. *Cancer Res.* **1987**, *47*, 6522−6527.
(46) Buettner, G. R.; Jurkiewicz, B. A. *Radiat. Res.* **1996**, *145*, 532−541.
(47) Chiou, S.-H. *J. Biochem.* **1984**, *96*, 1307−1310.
(48) Jin, Y.; Cowan, J. A. *J. Am. Chem. Soc.* **2005**, *127*, 8408−8415.
(49) Azab, H. A.; Banci, L.; Borsari, M.; Luchinat, C.; Sola, M.; Viezzoli, M. S. *Inorg. Chem.* **1992**, *31*, 4649−4655.
(50) Barrette, W. C. J.; Sawyer, D. T.; Fee, J. A.; Asada, K. *Biochemistry* **1983**, *22*, 624−627.
(51) Wood, P. *Biochem. J.* **1988**, *253*, 287−289.
(52) Borsook, H.; Keighley, G. *Proc. Natl. Acad. Sci. U.S.A.* **1933**, *19*, 875−878.
(53) Navaratnam, S.; Parsons, B. J. *J. Chem. Soc., Faraday Trans.* **1998**, *94*, 2577−2581.
(54) Bradshaw, R. A.; Peters, T. *J. Biol. Chem.* **1969**, *244*, 5582−5589.
(55) Lau, S.-J.; Sarkar, B. *J. Biol. Chem.* **1971**, *246*, 5938−5943.
(56) Cabras, T.; Patamia, M.; Melino, S.; Inzitari, R.; Messana, I.; Castagnola, M.; Petruzzelli, R. *Biochem. Biophys. Res. Commun.* **2007**, *358*, 277−284.
(57) Grogan, J.; McKnight, C. J.; Troxler, R. F.; Oppenheim, F. G. *FEBS Lett.* **2001**, *491*, 76−80.
(58) Harford, C.; Sarkar, B. *Biochem. Biophys. Res. Commun.* **1995**, *209*, 877−882.